

**SODIUM-SULFUR BATTERY :
ANALYSIS OF PERFORMANCE AND
CHARACTERIZATION OF BETA-ALUMINA
ELECTROLYTE**

By
SHIBAN KISHAN TIKU



**INTERDISCIPLINARY PROGRAM IN MATERIALS SCIENCE
INDIAN INSTITUTE OF TECHNOLOGY KANPUR**

JUNE 1974



SODIUM-SULFUR BATTERY:
ANALYSIS OF PERFORMANCE AND CHARACTERIZATION
OF BETA-ALUMINA ELECTROLYTE

A Thesis Submitted
In Partial Fulfilment of the Requirements
For the Degree of
MASTER OF TECHNOLOGY

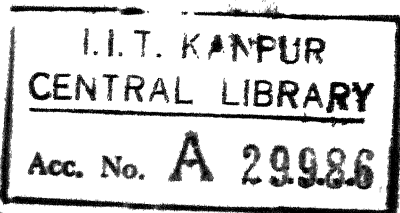
By

SHIBAN KISHAN TIKU

to the

Interdisciplinary Program in Materials Science
INDIAN INSTITUTE OF TECHNOLOGY KANPUR

JUNE 1974

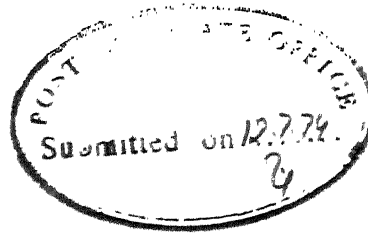


26 AUG 1976

Micro
62135
T449




MS- 1974-M-TIK-SOD



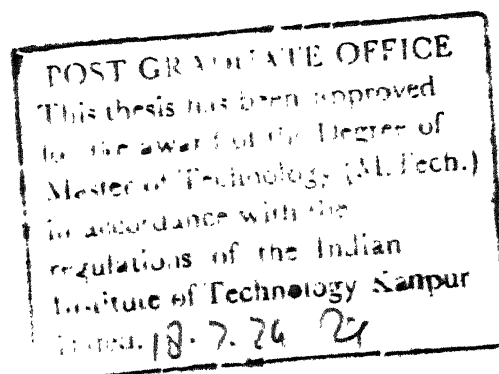
i.

CERTIFICATE

Certified that this work on "Sodium-Sulfur Battery:
Analysis of Performance and Characterization of
Beta-alumina Electrolyte" by S.K. Tikku has been
carried out under my supervision and that this has
not been submitted elsewhere for a degree.


(Dr. E.C. Subbarao)
Professor

Department of Metallurgical Engineering
Indian Institute of Technology
Kanpur.



ACKNOWLEDGEMENT

It has been a privilege to work with Professor E.C. Subbarao. I am grateful to him for his meticulous guidance throughout the work.

A large number of people have been of help directly or indirectly throughout my stay on the Campus, but it is not possible to name them all. I would particularly like to record my sincere thanks to the following: Messers A.K. Ray, C.B. Choudhary, H.S. Maiti, Bansilal, H. Jain, V. Velluri, V.K. Nagesh, M.K. Razdan and Vishwanath Singh.

Financial assistance from U.S. Air Force is gratefully acknowledged.

Finally, I wish to thank Mr. R.N. Srivastava for his excellent typing.

S.K. TIKU

CONTENTS

PART A

CHAPTER	PAGE
I INTRODUCTION	1
1. General	1
2. The Sodium Sulfur System	2
3. Inherent Advantages of the System	5
4. The First Laboratory Version	8
5. Recent Developments	11
6. Comparison With Other Systems	13
6.1 Advantages	13
6.2 Limitations	15
7. Operating Features	16
7.1 Operating temperature	16
7.2 Anode cathode volume changes	17
8. Components, the State of Art	17
8.1 Electrolyte	17
8.2 Carbon-sodium polysulfide electrode	18
8.3 Seals	19
8.4 Container materials	19
II STATEMENT OF THE PROBLEM	21
III ANALYSIS	22
1. Introduction	22
2. Assumptions	22
3. Performance	24
3.1 Average e.m.f. of a cell	24
3.2 Energy released in the reaction	24
3.3 Discharge efficiency	25
4. Single Tube Cell	28
4.1 Mass of the cell	28
4.2 Internal resistance of the cell	32
4.3 Results	32
5. Multitube Cell	32
6. Disc Type Battery	35
6.1 Total mass of the battery	36
6.2 Internal resistance	37
6.3 Specific energy	37
7. Preliminary Design of a General Purpose Vehicle Battery	38
7.1 General requirements	38
7.2 Mass of reactants	39
7.3 Dissipation	40
8. Discussion	40

PART B

CHAPTER	PAGE
IV SOLID ELECTROLYTE MEMBRANE	48
1.1 General	48
1.2 Empirical formula and synthesis	48
1.3 Crystal structure	49
1.4 Ionic conductivity	51
1.5 Ion exchange properties	52
2. Screening of the Electrolyte	54
2.1 Ionic conductivity measurement	54
2.2 Study of degradation	56
3. Aim of Experimental Work	57
V EXPERIMENTAL PROCEDURE	58
1. Fabrication of Material	58
1.1 Powder Preparation	58
1.2 Pressing	59
1.3 Sintering	59
1.4 Density	60
2. Conductivity Measurement	61
3. Sodium/Sodium Cell	63
4. Sodium Nitrate Electrolysis	65
5. Na/S Cell	66
VI RESULTS AND DISCUSSION	68
1. Conductivity Measurement - Results	68
1.1 Silver paint electrodes	68
1.2 NaNO ₃ liquid electrodes	71
1.3 Liquid sodium electrodes	71
2. Discussion of Conductivity Results	74
2.1 Electrode systems	82
2.2 Composition	84
2.3 Temperature	87
2.4 Frequency	89
3. Na/ β -alumina/Na Cell	91
4. Comparison of Electrode Systems	92
5. NaNO ₃ Electrolysis	94
6. Sodium-Sulfur Cell	94

PART C

SUMMARY AND CONCLUDING REMARKS	96
REFERENCES	98
APPENDIX	102

LIST OF FIGURES

FIGURE		PAGE
1.1	Schematic diagram of a sodium-sulfur cell (a) in comparison with that of a lead-acid cell (b) ³ .	4
1.2	Phase diagram of the Na_2S -S system ⁴	6
1.3	Variation of the e.m.f. of a Na/S cell with the variation of the melt composition ³	6
1.4	The first laboratory version of the sodium-sulfur cell ³	9
1.5	Typical charge-discharge curves for a 0.8 mm thick walled cell	10
1.6	Voltage-current density curves of a Na/S cell	10
3.1	Schematic diagram of a single tube cell	29
3.2	Schematic diagram of a proposed multi-tube cell	29
3.3	Schematic diagram of a flat plate battery	30
3.4	Single tube cell — variation of specific energy with wall thickness, electrolyte thickness and discharge time	43
3.5	Single tube cell — performance with variation in discharge efficiency and resistivity of electrolyte	43
3.6	Performance of a multitube cell with variation in diameter, and number of tubes as a parameter	44
3.7	Performance of a 100 tube cell with variation in discharge efficiency, length of tubes and cell wall thickness	45

FIGURE		PAGE
3.8	Performance of a flat plate battery	46
3.9	Sensitivity of the performance of a 12 cell stack to disc diameter, cell wall thickness and electrolyte thickness	47
4.1	Arrangement of ions in (110) plane of β -alumina crystal ⁷	50
4.2	Arrangement of ions in the [NaO] layer ⁷	50
4.3	Variation of electrical conductivity with temperature in single and polycrystalline β and β'' aluminas	53
5.1	Quartz sample holder for the silver paste measurements	62
5.2	Cell used for electrical conductivity measurement with liquid NaNO_3	62
5.3	Na/ β -alumina/Na cell schematic diagram	64
5.4	Cell for electrolysis of NaNO_3	64
5.5	Schematic diagram of the Na/S cell tested in the laboratory	67
6.1	The variation of the conductivity with temperature for samples A through E with silver paste and molten NaNO_3 electrodes at 1 MHz	70
6.2	Variation of conductivity with frequency (a) at 350°C, (b) at 400°C with molten NaNO_3 electrodes	73

CHAPTER	PAGE
6.3 Variation of the resistance of a Na/ β "-alumina/Na cell with time	75
6.4 Variation of the conductivity of a Na/ β -alumina/Na cell with temperature at $f = 1$ kHz and d.c.	75
6.5 Variation of the resistance with frequency — sodium electrodes	78
6.6 Impedance plots for Na/ β -alumina/Na cell (a) and its equivalent circuit (b)	79
6.7 Comparison of the conductivity vs. $1/T$ plots for sample D for the three electrode systems	80
6.8 Comparison of the frequency dependence of conductivity of β -alumina using NaNO_3 and Na electrodes at 350°C	81
6.9 Conductivity data of β -alumina measured with different electrode systems ²⁶	83
6.10 Comparison of the present conductivity data with the reported data	88

LIST OF TABLES

TABLE		PAGE
1.1	Estimated properties of electrical energy storage cells	14
5.1	Various compositions and their fired densities	60
6.1	Conductivity data with silver paste electrodes	69
6.2	Conductivity data for NaNO_3 electrodes at $f = 1 \text{ MHz}$	69
6.3	Variation of conductivity with frequency — molten NaNO_3 electrodes	72
6.4	Variation of $\text{Na}/\beta\text{-alumina}/\text{Na}$ cell resistance with temperature	76
6.5	Na electrode impedance data with frequency as a parameter	77
6.6	Reported conductivity measurements on $\beta\text{-alumina}$	85

SYNOPSIS

The thesis consists of three parts. In part A, the characteristics of a Na-S battery system are reviewed and an analysis of the performance of tubular and flat plate battery designs is described.

In part B, the heart of the battery system viz. the electrolyte, and its characteristics are briefly described. Characterization of the electrolyte material is critically reviewed. Five experimental samples of β and β'' alumina are evaluated using data obtained from experiments with three different electrode systems, over a range of temperatures and frequencies.

In part C, the results of the present work are summarized and some conclusions drawn.

CHAPTER I

INTRODUCTION

1. GENERAL

The prevalent energy crisis and the rapidly multiplying ecological problems have caused a grave concern all over the world. The dwindling conventional resources and the increased need to mitigate pollution have sparked a world-wide hunt for cleaner energy sources that are not dependent on fossil fuels. In case of the transportation systems, the major factors which are bound to bring change are: energy costs, air pollution, passenger handling capacity and impact of the system on natural resources.

The cost of energy from petroleum is going to increase. In contrast to this, central power station costs are predicted to decrease. Nuclear energy is projected to become a major contribution of energy near the end of the century; since this energy will be generated as electricity, the availability of such energy in future, should be an attraction for the design of electric vehicles and traction systems now. To make the power station power portable, good battery systems must evolve. In addition to mobile uses, batteries could be used for stationary uses, like large energy banks. The use of batteries is also anticipated to increase with the development of fuel cells and solar cells, as their advantages can be fully exploited in hybrid systems needing storage batteries.

Several reviews have assessed the candidate battery systems which could be considered for general purpose vehicle systems^{1,2}. Only high energy battery systems can result in a viable power system for a general purpose vehicle. None of the currently available battery systems fulfills both the high energy and the high power density requirements. High temperature batteries are attractive for traction applications because they offer both high power density and high energy density. High energy density is achieved by selecting reactants of low equivalent weight and high electronegativity difference. High power capability is attained by: increasing the exchange current density through the use of one or more components in liquid form, achieved by operating the system at elevated temperature, and by using low resistance electrolyte.

The sodium-sulfur system is a particularly attractive system belonging to this class of high temperature, high energy batteries. It has attracted the attention of more organizations than any other system because it has the greatest potential for meeting the requirements for an electric car. The system is ideally suited for an underground energy bank.

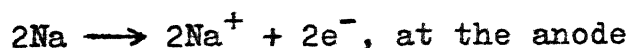
2. THE SODIUM-SULFUR SYSTEM

The great interest in the sodium-sulfur storage battery, using beta-alumina as the electrolyte, is due to the fact that the characteristics of the anodic and cathodic reactants allow one to expect batteries with an energy density higher than

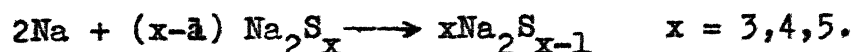
150 W-hr/kg., under satisfactory economic conditions. This fact makes the sodium-sulfur battery one of the most promising portable power sources.

This cell, originally proposed by Kummer and Weber of the Ford Motor Co., (1967)³ is a product of the interaction of fundamental research in solid-state science and a continuing awareness of the energy problem. The cell makes use of a revolutionary approach to the battery problem, that of using liquid electrodes and separating them by a sodium-ion conducting solid membrane of beta-alumina — using a solid electrolyte. The schematic diagram of the cell is shown in fig. 1.1a and that of a common lead- acid battery in fig. 1.1b for comparison. In the latter case, electrons pass through the external circuit where they do work, and ions through the H_2SO_4 electrolyte to complete the reaction, which is essentially the oxidation of lead and reduction of lead dioxide. The reactants and products are solid and the electrolyte liquid.

The reactions in the sodium-sulfur cell are:



The sulfur rich polysulfides formed at first react with sodium to give polysulfides richer in sodium:



The operating temperature is dictated by the temperature at which the product can be retained in a liquid state. Thus

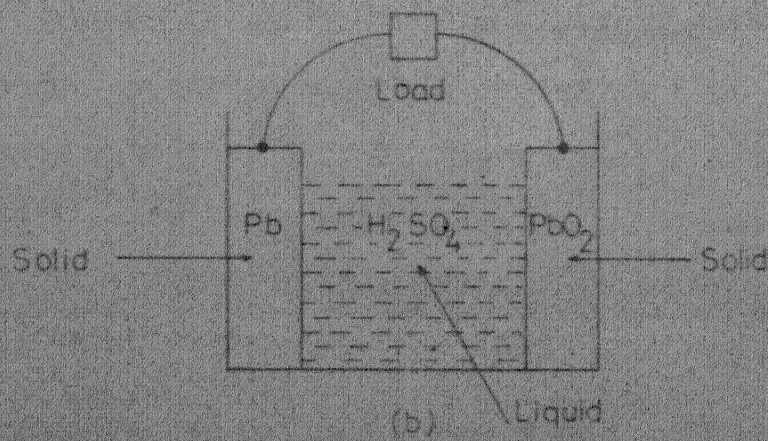
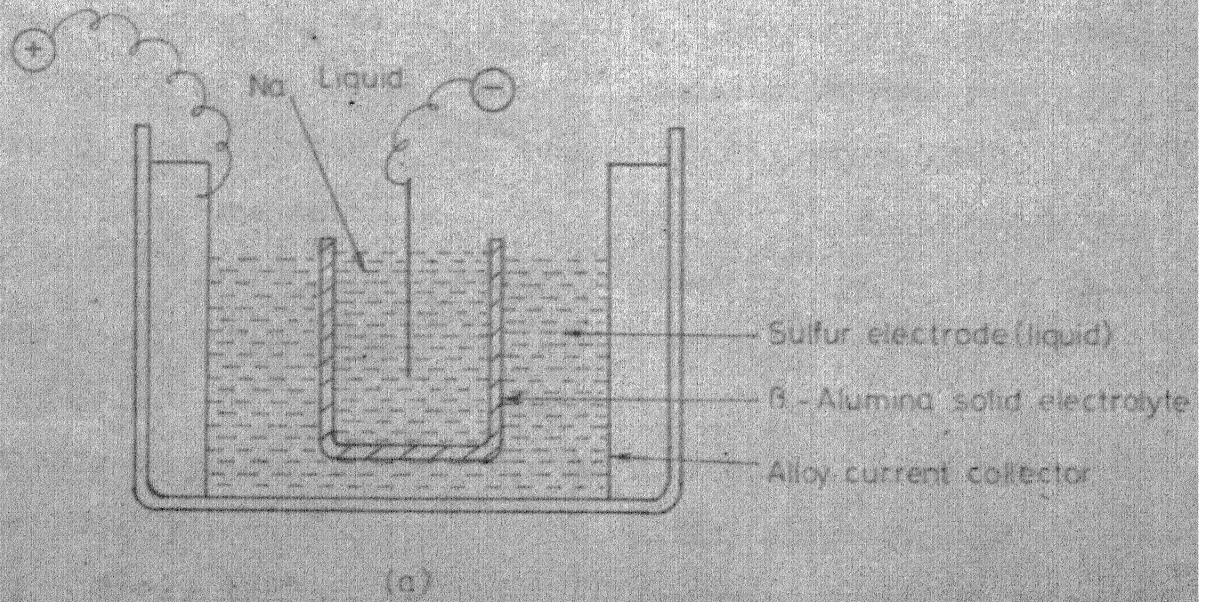


Fig. 1.1: Schematic diagram of a sodium-sulfur cell (a) in comparison with that of a lead-acid cell (b)

the imposed constraints can be found from a phase diagram. The phase diagram of the Na_2S -S system, shown in fig. 1.2, has been proposed by Gupta and Fischer⁴, revising the one proposed by Pearson and Robinson⁵. The temperature at which the sulfur-polysulfide melt can be retained in a liquid phase sets up the lower limit on the working temperature. At a temperature of 300°C , solid begins to separate out at a composition near that of Na_2S_3 . At 350°C , the composition $\text{Na}_2\text{S}_{2.7}$ would be the limit. In practice, however, the Na_2S_3 composition is taken as the 100% discharged state. The melting point of Na_2S_3 , viz. 275°C , and the boiling point of sulfur, viz. 444°C , hence set the lower and upper limits to the operating temperature of a sodium-sulfur cell.

The free energy of formation of Na_2S_5 is about 96 Kcal/mole⁴ at 300°C and the corresponding e.m.f. is 2.08V. Hence for a melt rich in sulfur, the e.m.f. of the couple is 2.08V. The variation of the e.m.f. of a sodium-sulfur cell with the variation of the composition of the melt is shown in fig. 1.3. Starting with pure sulfur, the voltage remains constant till a composition corresponding to Na_2S_5 is reached. It then drops almost linearly to 1.76V, when melt composition corresponds to Na_2S_3 , which is taken as the 100% discharged state.

3. INHERENT ADVANTAGES OF THE SYSTEM

The heart of the sodium-sulfur battery is the beta-alumina solid electrolyte. Since beta-alumina can be made to

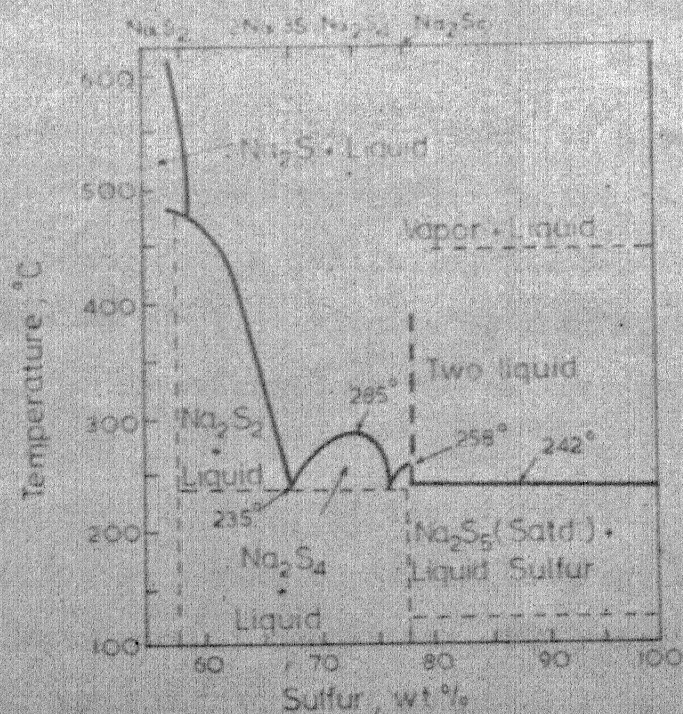


Fig. 1.2: Phase diagram of the Na_2S -S system⁴

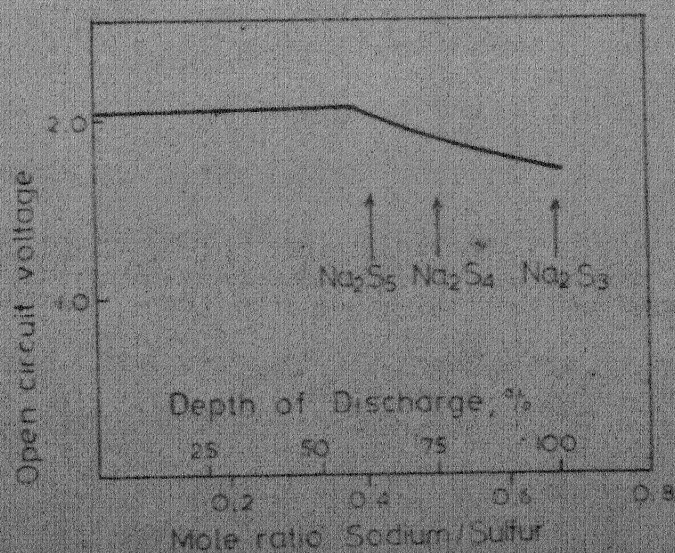


Fig. 1.3: Variation of the e.m.f. of a Na/S cell with the variation of the melt composition⁵

conduct a range of species^{6,7}, there is a choice in the selection of the anode material. Sodium is selected because it is cheap and easily available, its melting point is low and because sodium beta-alumina is easy to fabricate.

Sulfur is selected as the cathode material, because it is inexpensive and plentiful, is in liquid state at only 115°C and the formation energy of the polysulfides is quite high, which results in a high theoretical energy density of the system. Under proper conditions, the reaction between sodium and sulfur is electrochemically reversible, thus making the battery rechargeable. The polysulfide melt can be retained in a liquid state at a relatively low temperature compared to other sodium salts. Sulfur is a poor electronic conductor, but this problem is easily solved by holding it in graphite. The polysulfides of sodium are semiconducting materials, hence their accumulation does not affect the cathode reaction.

The reactants and products being liquid, the cell reaction is fast, allowing high current densities. The reactants can be regenerated in the same physical form during recharging because they are in liquid form, thus making repeated charge-discharge cycling possible. In solid reactant systems cycle life is limited due to this fact. The cell reaction is simple and involves no gaseous products. Side reactions can not take place in the system thus ruling out the possibility of self-discharge.

The highest vapor pressure encountered in ~~the system~~¹⁰ would be the vapor pressure of sulfur, viz. ~ 60 mm of Hg at 300°C . Common materials can be used as containers. Stainless steel has been found to be quite satisfactory.

4. THE FIRST LABORATORY VERSION

The small laboratory cell, developed by Weber and Kummer³ is shown in fig. 1.4. The cell, enclosed in a sealing glass envelope, used the stabilized β'' -alumina, with a resistivity of 5 ohm-cm. at 300°C , as the electrolyte. The ceramic was in the form of a thin walled tube to which a sodium reservoir was sealed at the top. Surrounding the tube was the sulfur electrode — a 3 mm thick layer of carbon felt, holding the liquid sulfur by capillary forces. The graphite electrode was backed by an alloy current collector while a wire dipped in the liquid sodium acted as the anode current collector.

Typical charge-discharge curves for this cell, having a 0.8 mm thick ceramic electrolyte are shown in fig. 1.5. The voltage-current density relations drawn in fig. 1.6 are essentially straight lines and show the absence of overvoltages due to slow reaction or slow mass transfer — activation or concentration polarization. Results obtained with small laboratory cells proved that the sodium-sulfur system was a very promising one.

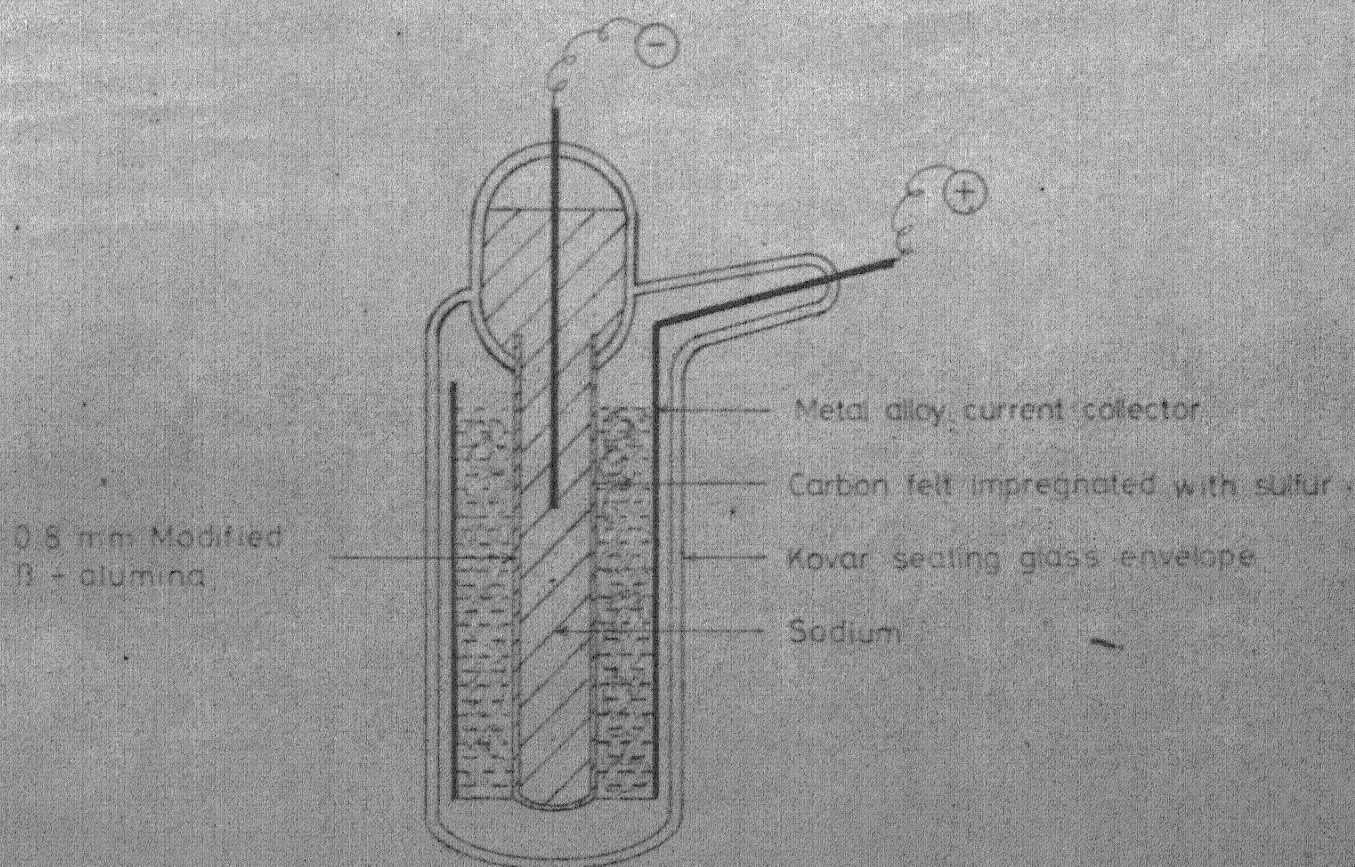


Fig. 1.4: The first laboratory version of the sodium-sulfur cell³

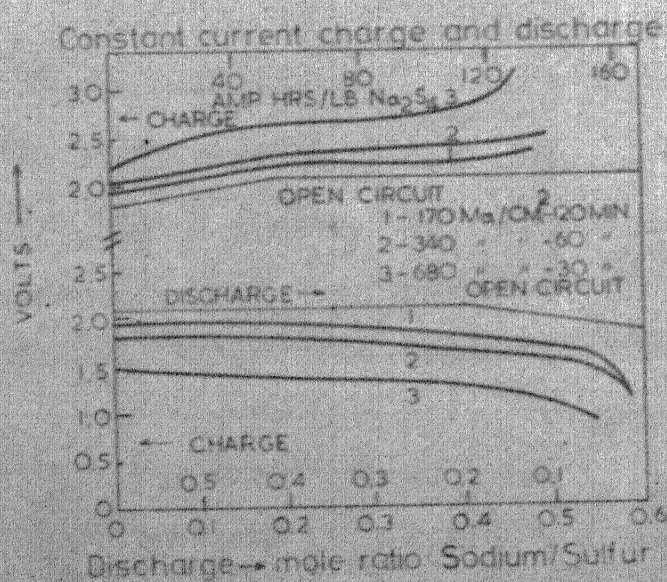


Fig. 1.5: Typical charge-discharge curves for a 0.8 mm thick walled cell

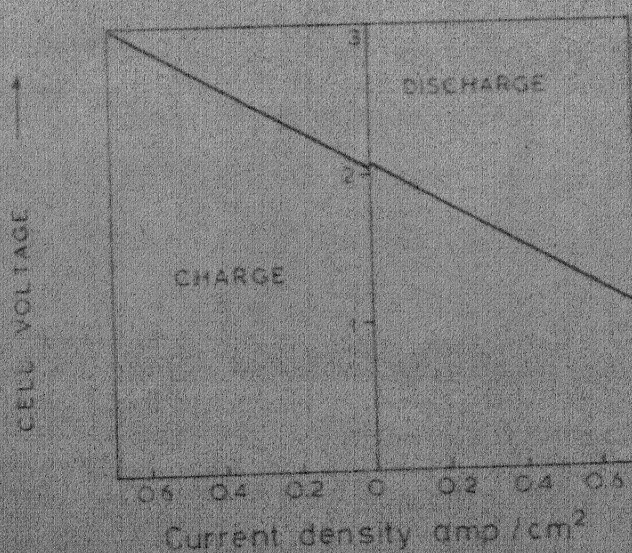


Fig. 1.6: Voltage-current density curves of a Na/S cell

5. RECENT DEVELOPMENTS

The early promise of the sodium-sulfur cell has not fully materialized so far. The problem areas in the design and operation of the cell are resistivity of the solid electrolyte, electrode polarization, corrosion of cell materials, degradation of solid electrolyte after frequent charge-discharge cycles and the operating temperature. Work is continuing towards solving these problems in U.S.A.^{8,9}, Britain¹⁰⁻¹³, Japan, France¹⁴⁻¹⁷, U.S.S.R.¹⁸ etc.

The Ford Motor Co., the pioneers of the sodium-sulfur cell, have not come up with a completely practical battery till now. In Britain, the British Railways started to develop a practical battery for their traction system. They have developed and tested tubular as well as flat plate battery designs^{10,12}. They have standardized on a working temperature of 350°C. The tubular cell arrangement was adopted for initial experiments because in this design, the sealing area between the electrolyte and the cell wall could be kept to a minimum. A number of single tube and multiple tube cells were constructed and specific energy of 400 W-hr/kg was achieved. The flat plate batteries were designed for high rate systems (discharge time \leq 1 hr). The longest life achieved at a current density of 120 mA/cm² was continuous 1000 hours, consisting of 400 cycles of charge-discharge.

Tests were reported by Electricity Council Research Centre (G.B.) on cells of about 45 Ahr capacity, which gave

erratic performance and failed early due to beta-alumina diaphragm break-down¹³. Life times of over 5000 hours have now been achieved by this group¹⁹ in continuous charge-discharge cycle tests (4 cycles/day); where the maximum discharge current is restricted to 200 mA/cm^2 and maximum charging current to 100 mA/cm^2 .

Stainless steel cells were constructed in France^{14,15}, and the break-down of the electrolyte prevented by controlling the rate of re-charge. This group has studied the mechanism of degradation of electrolyte, and gathered evidence to prove that magnesia additions and presence of contaminants result in the reduction of life-time of the beta-alumina electrolyte¹⁶. This group has standardized a fusion synthesizing method for beta-alumina electrolyte and has used electrophoresis to make thin, closed-end beta-alumina tubes¹⁷.

An alternative approach to increase the operating life of the system is to decrease the working temperature and this was tried in U.S.A.²⁰ by the addition of aluminum polysulfides to the sodium polysulfide melt. An electrode material with a melting point of 200°C was achieved. This also permits sealing with taflon.

The Ford Motor Co., seems to have solved the cycle life problem, as they have achieved a life greater than 2000 cycles in their cell designs⁸. A systematic study of the problems associated with the system has been undertaken. The degradation of the electrolyte has been studied and methods to avoid ceramic

cracks — by optimization of material composition and fabrication^{21,22} — have been developed. A 12 volt battery of 24 tube cells, connected to give four parallel sets, each containing 6 cells in series, has been tested⁹. The battery, designed for 250 W, was tested for 300 W and gave peak power of 400 W for short durations. A reversible capacity of 15 A-hr was found, compared to the theoretical capacity of 20A-hr.

The electrical performance of individual cells has been very encouraging. Cells designed to be identical gave variation in amp-hr capacity and internal resistance. Due to this unbalance, a string of cells in series shows a loss of performance. The sensitivity to unbalance is greatly reduced when cell strings are connected in parallel.

More work is needed to improve electrolyte life and cell reliability before multi-kilowatt batteries can come into the market.

6. COMPARISON WITH OTHER SYSTEMS

6.1 Advantages

The achieved or projected performance characteristics of some of the battery systems are shown in table 1.1. The sodium-sulfur battery uses a moderately high temperature, and yet gives a high specific energy and power. The theoretical specific energy of the system is 762 W-hr/kg, compared to a value of 192 W-hr/kg for the lead-acid battery. It is believed, however, that a value of 330 W-hr/kg can be easily achieved for

Table 1.1

Estimated Properties of Electrical Energy Storage Cells

Cell	Typical Temp. °C	Resistivity of Electrolyte ohm-cm.	Cell voltage at discharge volts	Current density, A/cm ²	Specific Power W/kg	Specific Energy, W-hr/kg	Operating life cycles
Lead-acid	40-50	1.53	2.1-1.46	0.01	7-30	4-33	10-400
Ni-Fe	0-40	1.96	1.3-0.75	-	7-40	30-35	100-3000
Ni-Cd	40-60	1.96	1.3-0.75	0.01	7-44	35-40	100-2000
Ag-Zn	0-40	1.96	1.55-1.1	0.45	24-150	80-100	100-300
Ag-Cd	40-60	1.96	1.3-0.8	-	20-66	50-60	500-1100
Li-Cl ₂	650	0.17	3.40	1-3	80-150	330	-
Li-Te	450-480	0.26	1.79-1.67	2-5	280	180	-
Na-Air	130	3.58	2.3	0.07	90	350	-
Na-Bi	540-580	0.44	0.8-0.44	0.5-1	80	40	500
Zn-Air	25	-	1.4	-	60	200-300	300-400
Na-S	300	5	2.08-1.76	0.7	330	330	2000

practical systems while only 5-30 W-hr/kg is achievable for the lead-acid system.

The system gives energy densities comparable to the high energy density systems such as lithium-chlorine, which require a higher operating temperature, and involve more severe materials problems.

The system uses an impervious ceramic as electrolyte, hence there is no chance of diffusion of reactants through the electrolyte that would result in self-discharge. The cells are capable of yielding very high current densities ($\sim 400 \text{ mA/cm}^2$). The batteries can be recharged at a high efficiency even at very high charging rates.

6.2 Limitations

The limitations of the system are summarized below:

- i) High temperature is required for operation which necessitates^t use of a thermal shield. In case, a battery cools below the operating temperature, it has to be heated to a temperature beyond 300°C for restarting. Hence heating coils are needed in addition to thermal insulation for intermittent operation, and these will increase the bulk of the system.
- ii) The internal resistance of the presently fabricated cells is high, and this limits the current density.
- iii) The most severe problem is the short life of the electrolyte in terms of the number of charge-discharge cycles.
- iv) The durability of the seals and cathode current

collector under the working conditions is a limitation.

v) Ceramics are sensitive to mechanical and thermal shock and thermal cycling.

vi) The present designs of the battery are not safe and reliable. Breakdown of the electrolyte can cause mixing of the reactants and lead to an explosion. When used in mobile equipment a calamity can occur in case of an accident. Thus the packaging of the battery is a challenging engineering problem.

7. OPERATING FEATURES

7.1 Operating Temperature

A number of factors must be considered in choosing the operating temperature of the battery system. To allow for large temperature excursions, the operating temperature should be in the middle of the available range, i.e., about 350°C , considering 275°C and 444°C as the lower and upper limits respectively. With increase in temperature, the performance of a battery should improve, because the solid electrolyte resistance is lowered and mass transfer in the sulfur electrode becomes faster. A higher operating temperature would be desirable in view of the above. This is, however, offset by the fact that the corrosion rate increases with temperature. Thus, in order to achieve a reasonable life, the operating temperature must be kept low. Hence, until good corrosion resistant materials are found, the temperature of operation

must be limited to 300°C.

7.2 Anode-Cathode Volume Changes

Volume changes within a cell can take place because of a variety of reason: thermal expansion, depletion or creation of material and phase changes or product formation. These changes must be accounted for in the design of a battery. Since the densities of sulfur and the sodium polysulfides melts ~~are~~ nearly the same, about 40 percent increase in volume takes place on complete discharge in the cathode chamber. On the other hand, the volume of sodium decreases linearly with the depth of discharge and the incorporation of a porous wick can ensure that sodium is brought to the electrolyte surface.

8. COMPONENTS, THE STATE OF ART

8.1 Electrolyte

Fally et al¹⁶ have shown that the presence of impurities and MgO additions are responsible for low cycle life. This group has therefore standardized use of pure β -alumina. The Ford Motor Co. claims to have solved the life-time problem. They have investigated ceramic compositions to optimize durability, ease of fabrication and electrical properties*. On the basis of screening tests developed by them, the composition 9.25% Na_2O - 0.25 Li_2O - rest Al_2O_3 has been found to be superior to all other compositions tested.²¹

* Covered by U.S. Patents (not available).

Presently discs with resistivities of 4-15 ohm-cm. and cell life of at least 3000 hours with current reversal at 0.2-0.25 A/cm² can be produced consistently in the laboratory.

8.2 Carbon-Sodium Polysulfide Electrode

The conductivity of sodium-polysulfide melts have been measured.²³ The total cell internal resistance remains approximately constant over the composition range S to Na₂S₃. Experiments have demonstrated that this electrode is highly reversible with very high exchange current densities⁸. Therefore, the reaction at this electrode is not likely to become the rate-determining step. However, the complex set of chemical reactions, preceding and following the electron transfer step, combined with the high resistivity of sulfur, may result in mass transport limitations. Experimental studies have demonstrated that these limitations may become significant depending upon the size and shape of the cathode.

In the charging process, higher sulfides and sulfur are formed which subsequently equilibrate with the bulk of the sulfide phase by chemical reaction and diffusion until a sulfur saturated Na₂S₅ melt is formed with any additional sulfur remaining as a separate phase. During discharge, lower sulfides are formed which equilibrate with the bulk of the melt and take up more sulfur, until the melt composition reaches the liquidus line in the phase diagram and the solid Na₂S₂ no longer dissolves in the melt. Establishment of a

sulfur electrode design capable of minimizing concentration polarization is necessary.

8.3 Seals

The life-time of a Na-S battery depends on the durability of the seal used. In addition to being passive to the cell reactants and products, the seal must have: high electrical resistance, thermal expansion coefficient approximately equal to the ceramic, mechanical strength and resistance to thermal cycling.

Seal materials and techniques using a borosilicate glass frit are being developed for sealing electrolyte to the insulating ceramic. Polymeric adhesives, glass sealing and brazing have been used to seal the insulating ceramic to the metal container⁸.

8.4 Container Materials

Cheap, light-weight and corrosion resistant materials are required for containers. Corrosion studies have been done on possible container, backing electrode and connector materials. A number of stainless steel and nickel base alloys have been tested and found satisfactory, as they form protective sulfide layers. These layers, however, give rise to a large resistance which is undesirable in the case of backing electrodes.

Although, the results so far obtained establish the advantages of the Na-S battery concept, further research must be

carried out before a practical battery with sufficient life time and reliability can be built.

CHAPTER II

STATEMENT OF THE PROBLEM

The primary aim of the present work was to investigate the possibility of using beta-alumina prepared in this laboratory for the fabrication of a sodium-sulfur cell. Concurrently, it was thought worth while checking which parameters are critical in determining the performance of this cell and what are the essential properties required of an electrolyte material to be used in the cell. Since other research groups have had problems associated with the life-time of the high conductivity beta-alumina, a need exists for the determination of the amount of electrical conductivity that can be sacrificed to achieve improved performance regarding cycle life. Analysis of various battery configurations was taken up with this view.

CHAPTER III

ANALYSIS

1. INTRODUCTION

Several factors must be considered when applying a battery system to a practical application. For mobile use, the factors are: performance, operational features, impact on traction system design, cost, safety and durability. For stationary use, such as an energy bank, the overall bulk may not be a constraint but optimization of performance is still important.

The performance of a battery depends upon the discharge efficiency and the discharge rate*. Knowing the internal resistance of the battery and the dimensions, one can calculate the performance of the battery i.e., the variation of energy density and power density with discharge time and discharge efficiency as parameters. Using internal resistance data obtained in the laboratory, these calculations can be done using a digital computer. Employing many relevant combinations of parameters, results can be used to determine interactions between component dimensions, operating conditions and cell characteristics.

2. ASSUMPTIONS

In performing these calculations, the following assumptions have been made unless otherwise stated.

(* See appendix for definitions).

i) Conversion to Na_2S_3 is taken as 100% discharge. Energy released is calculated from the free energy change associated with the formation of Na_2S_3 . In practice the percentage utilization of sulfur is less than 100%. This is more pronounced during the first few cycles ($\sim 85\%$) and in tubular cells.

ii) The ionic conductor has a negligible electronic conductivity, so that the current efficiency can be taken as 100%.

iii) The internal resistance of the cell is ohmic. Constant resistance is shown by cells upto a current density of 500 mA/cm^2 .³ (fig. 1.6).

iv) The cell internal resistance is independent of the state of discharge. (fig. 1.3).

v) The operating temperature is taken as 300°C .

The assumptions can not be true under all the operating conditions. It has been found, however, that assumption (i) is valid upto a current density of 500 mA/cm^2 , at least for the flat plate design. For the tubular design the cell internal resistance has been taken as given by $r = 0.5 + 5t$ (ohm-cm^2), where t is the thickness of the electrolyte; because of the fact that the sulfur electrode resistance can not be calculated accurately because of the complicated geometry. For flat-plate cells the internal resistance r is taken as given by

$$r = \rho_{se} t_{se} + \rho_{\beta} t$$

The symbols used are defined below

The resistivity of sulfur electrode = $\rho_{se} = 10 \text{ ohm-cm}^*$

$\rho_{\beta} = 5 \text{ ohm-cm}$, unless otherwise specified.

t_{se} = thickness of sulfur electrode

t = thickness of electrolyte.

The resistance of Na/ β -alumina interface has been neglected as this has been proved to be negligible³¹.

3. PERFORMANCE

3.1 Average e.m.f. of a Cell

The e.m.f. of a Na-S cell stays constant at 2.08V upto a depth of discharge of about 60% and then falls linearly to a value of 1.76V at 100% discharge. (see fig. 1-3).

Hence the average e.m.f.

$$E_{av} = 0.6 \times 2.08 + 0.40 (1.76 + 2.08)$$

$$E_{av} = 2.016 \text{ Volts.}$$

3.2 Energy Released in the Reaction

The free energy change associated with the reaction can be obtained using the Gibbs-Helmholtz eqn.

$$Q/nF = E - T \left(\frac{\partial E}{\partial T} \right)$$

at constant T, $Q = EnF$

where $F = 23,070 \text{ farads}$

* order estimated from
 i) Sudworth¹²
 ii) Minck⁹

$n = 2$ (as two electrons are transferred for the formation of one molecule of any polysulfide).

$$\begin{aligned}\text{Therefore } Q &= 2.016 \times 2 \times 23,070 \\ &= 93.01 \text{ Kcal/mole}\end{aligned}$$

$$\text{or } Q = 762.8 \text{ W-hr/kg of Na}_2\text{S}_3 \text{ (product)}$$

$$\text{or } Q = 762.8 \times \frac{32 \times 3 + 23 \times 2}{32 \times 3} \times 10^{-3} \text{ W-hr/gm of S.}$$

$$\text{Therefore } G = Q = 1.125 \text{ W-hr/gm of S.}$$

3.3 Discharge Efficiency

Let us consider a cell containing m gms. of sulfur. (The corresponding amount of Na for the product at 100% discharge to be Na_2S_3 is therefore $m/2.1$ gms). Let the internal resistance be R_{in} , so that when a current I is drawn the average output voltage is

$$V_o = E_{av} - R_{in} I$$

Power consumed in the load

$$P_o = I[V_o] = I(E_{av} - R_{in} I)$$

Assuming a discharge time of T hours the energy consumed in the load $= IT[E_{av} - R_{in} I]$.

$$\begin{aligned}\text{Now, packed energy in the cell (based on mass of sulfur)} &= \\ &= mG(\text{W-hr})\end{aligned}$$

(where m is in gms, G is in W-hr/gm).

Amp. hours spent in the load and internal resistance = mG/E_{av} .

Assuming a discharge time of T (hours) average current = $I = \frac{mG}{E_{av}T}$

$$\text{Power in the load} = I \cdot V_o$$

$$= I[E_{av} - R_{in}I]$$

$$\text{or } P_o = \frac{mG}{E_{av}T} [E_{av} - \frac{R_{in} mG}{E_{av}T}]$$

$$\text{Energy consumed in the load, } W_o = P_o T$$

$$= mG[1 - \frac{R_{in} mG}{E_{av}^2 T}]$$

$$\text{Discharge efficiency based on packed energy, } \eta_d = \frac{W_o}{mG}$$

$$\text{or } \eta_d = 1 - \frac{R_{in} mG}{E_{av}^2 T}$$

For a specific cell,

$$\eta_d = 1 - C/T$$

$$\text{where } C = \frac{R_{in} mG}{E_{av}^2} \text{ is a constant.}$$

To calculate the watt-hour efficiency of a cell in operation where it is charged electrically, the energy needed to charge to 100% charged state can be calculated assuming same internal resistance and charging time, T_{ch} hours. In a similar manner the watt-hr efficiency would be given by

$$\eta = \frac{1 - C/T}{1 + C/T_{ch}}$$

In Na-S cells the current density during charging is limited to a considerably lower value than that during discharging, because the life of the electrolyte is critically dependent upon the current density during charging. Here only discharge efficiency η_d is considered because the energy lost during charging is not important, what is important is 'How much of the packed energy is usefully employed during discharge'. Hence

$$\eta_d = 1 - \frac{R_{in} mG}{T E_{av}^2} \quad \dots (1)$$

will be taken as the parameter.

$$\text{Also } W_o = mG \eta_d \quad \dots (2)$$

3.4 Specific Energy

Specific energy is given by

$$W_s = W_o/M,$$

where M is the total mass of a cell or battery. Here, the mass of accessories is not considered, and M will be calculated in terms of m, the mass of sulfur, which is dependent upon the operating parameters η_d and T,

From eq. (1)

$$m = \frac{(1 - \eta_d) T E_{av}^2}{R_{in} G} \quad \dots (1a)$$

$$\text{Also } W_s = W_o/M = mG \eta_d/M \quad \dots (3)$$

Specific energy will now be calculated for tubular and flat plate cells, starting with the simple case of a single tube cell.

4. SINGLE TUBE CELL

The proposed geometry of a single tube cell is shown in fig. 3.1. Let us assume:

active tube length = L (cms)

average diameter of the tube = d (cms)

thickness of the tube = t (cms)

and thickness of cell wall = t_w (cms)

4.1 Mass of the Cell

The mass M of the cell is given by the sum of the masses of the various components.

$$M = \text{mass of sulfur} + \text{mass of sodium} + \text{mass of graphite} \\ + \text{mass of electrolyte} + \text{mass of outer casing} \\ + \text{mass of accessories (leads, seals etc.)}$$

The mass of the accessories will be neglected in the computation, as this will not cause much change in the performance. For a practical system, other accessories such as thermal insulation and heating coils are needed, and these must be accounted for in estimating the performance.

The masses of the various components are calculated in terms of the mass of sulfur, m .

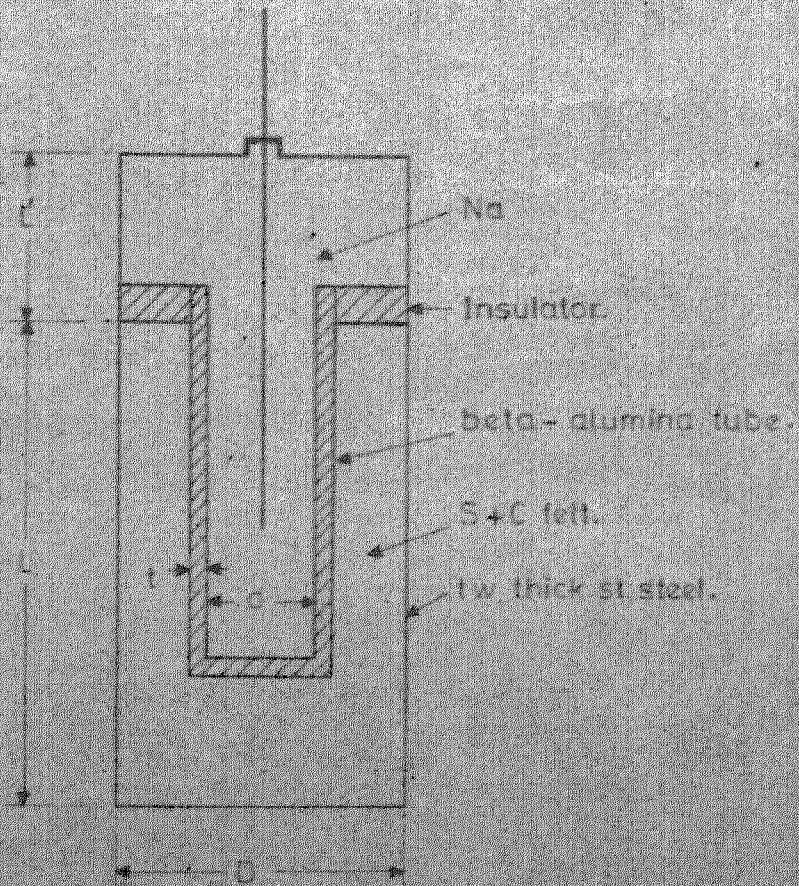


Fig. 3.1: Schematic diagram of a single tube cell

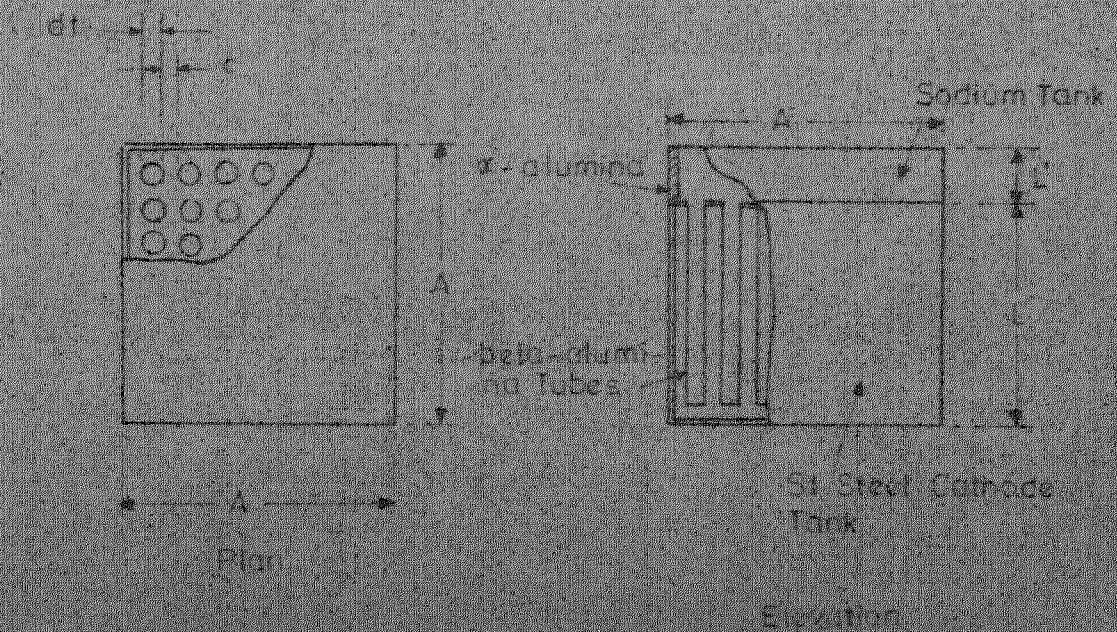


Fig. 3.2: Schematic diagram of a proposed multi-tube cell

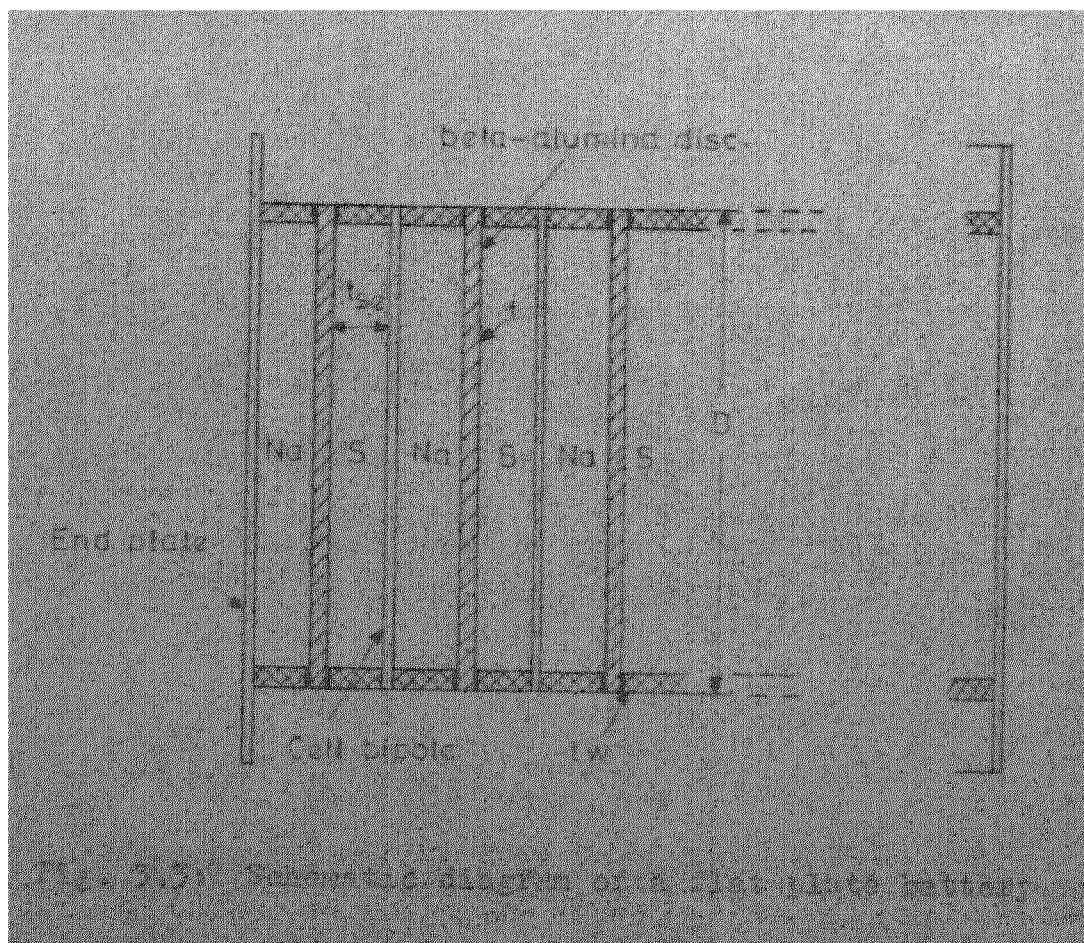


Fig. 2.3: Schematic diagram of a flat plate battery.

a) Sodium

To maintain constant level of sodium in the tube with discharge, some excess sodium must be taken in the reservoir.

$$\begin{aligned}\text{Ideal mass of sodium} &= m/2.1 \text{ (gms)} \\ &= 0.476 m\end{aligned}$$

$$\text{Volume of electrolyte tube} = \frac{\pi}{4} \times d^2 \times L$$

$$\text{Therefore mass of excess sodium} = 0.88(\pi \times d^2 \times L/4)$$

$$\text{Total mass of sodium} = 0.476 m + 0.692 d^2 L$$

b) Carbon-felt

$$\text{Mass of product} = m + 0.476 m = 1.476 m$$

$$\text{Density of product} = 1.86 \text{ (gm/cc)}$$

$$\therefore \text{Volume} = 1.476 m / 1.86$$

Considering carbon felt of 97% porosity, the volume of the cathode

$$= \frac{1.476 m}{0.97 \times 1.86} = 0.818 m$$

$$\text{Density of carbon felt} = 0.085 \text{ (gm/cc)}$$

$$\therefore \text{Mass of carbon felt} = 0.818 \times 0.085 m$$

$$= 0.0695 m.$$

c) Electrolyte

$$\text{Volume of } \beta\text{-alumina} = \pi \cdot d \cdot L \cdot 1.05 t$$

(Assuming 5% extra length and neglecting the base of the tube)

$$\begin{aligned}\text{Mass of Electrolyte} &= 3.2 \times \pi dL \times 1.05 t \\ &\approx 10 d L t\end{aligned}$$

d) Stainless Steel Case

Knowing the volume of the cathode (0.818 m), the diameter of the cell case is found to be given by

$$D = (1.043 m/L + d^2)^{\frac{1}{2}}$$

Using 7.75 gm/cc as the density of the stainless steel, the mass is given by

$$\begin{aligned}\text{mass of case} &= 7.75 \pi L t_w D \\ &= 24.35 L t_w D\end{aligned}$$

Neglecting the mass of the insulating separator, and knowing the mass of sodium to be contained [= m/(2.1 x 0.88)] the mass of the sodium tank can be calculated.

The overall mass of the stainless steel

$$= 24.35 L t_w D + 2.165 t_w m/D + 12.2 t_w D$$

Taking the sum of all the masses, the overall mass of the single tube cell is given by

$$\begin{aligned}M &= 1.55 m + 0.692 d^2 L + 10 d L t + 24.35 t_w D \\ &\quad + 2.165 t_w m/D + 12.2 D^2 \quad \dots (4)\end{aligned}$$

where $D = (1.043 m/L + d^2)^{\frac{1}{2}}$

4.2 Internal Resistance of the Cell

The internal resistance will be assumed to be given by

$$R_{in} = r/\text{Area} \quad (5)$$

$$\text{where } r = 0.5 + 4 t$$

$$\text{and Area} = \pi d t.$$

4.3 Results

Taking the following data, the specific energy of the cell is calculated as a function of the various parameters, using eqns. (1) - (5).

Tube diameter, d	= 1.0 cm
Cell wall thickness, t_w	= 0.04 cm
Effective length, L	= 15.0 cm
Electrolyte thickness, t	= 0.1 cm
Discharge time, T	= 1 hour
Discharge efficiency η_d	= 0.75
Electrolyte resistivity, ρ	= 4 ohm-cm.

The performance is shown in fig. 3.4, where variation of the specific energy with electrolyte thickness, wall thickness and discharge time has been plotted. Fig. 3.5 shows the performance with variation in discharge efficiency and electrolyte resistivity at thicknesses of 0.1 cm and 0.2 cm.

5. MULTITUBE CELL

The proposed geometry of a multitube cell is shown in

fig. 3.2* Some further assumptions made in this case are:

i) The cell case cross-section is taken as a square, which has the minimum perimeter for a given area. The side of the square is just large enough to accommodate \sqrt{N} tubes with clearance.

ii) The minimum clearance between the electrolyte tubes is taken as 0.2 cm and that between tubes and cell walls as 0.1 cm.

iii) The sodium reservoir is assumed to consist of a 3 mm thick, α -alumina tank, with the β -alumina tubes sealed to its base.

iv) Dead space at the bottom and the accessories are again neglected.

Proceeding as in the single tube case, the overall mass of the cell is given by:

$$M = 1.55 \pi + 0.6908 \ln(d_t - 2t)^2 + 7.75 t_w [A(4L + A)] + 2.56 m/A. \quad \dots (6)$$

where the tank dimension is:

$$A = \left[\left(\frac{0.818 m}{NL} + 0.785 d_t^2 \right) N \right]^{\frac{1}{2}} \quad \dots (7a)$$

The clearance between the tubes is:

$$c = A/\sqrt{N} - d_t$$

In case c turns out to be less than 0.2 cm (using eq. (7a)), it is taken as 0.2 cm and correspondingly the expression for A gets modified to:

* Refer to this diagram for nomenclature.

$$A = (dt + 0.2)\sqrt{N} \quad (7b)$$

The internal resistance of the cell is:

$$R_{in} = (5t + 0.5)/N \pi d_t L \quad (8)$$

Using eqns. (1) - (3) and (6) - (8) the performance of a multitube cell has been evaluated and is shown in figs. 3.6 and 3.7. The data used are given on the diagrams.

6. DISC TYPE BATTERY

Disc type geometry can result in a high voltage and high rate battery. A schematic diagram is shown in fig. 3.3. In this case, the electrode geometry is clearly defined and the variation of the sulfur electrode resistance can be allowed for. As the sulfur electrode resistance increases, there is a small change in the resistivity of the electrode, this change is neglected in the calculations that follow. Again, the variation in resistance with the state of discharge is neglected.

The important component dimensions are: electrolyte disc diameter, disc thickness and cell wall thickness. The thickness of the sulfur and sodium electrodes depend on the discharge efficiency and the discharge time and these two, therefore, have a marked effect on the performance of the battery.

Nomenclature:

Diameter of electrolyte disc	=	D	
Thickness of electrolyte	=	t	
Number of cells	=	N	
Thickness of cell wall	=	t_w	
Thickness of bipole	=	t_{bp}	= 0.04 cm (assumed)
Thickness of end plates	=	t_{ep}	= 0.15 cm (assumed)
Thickness of sulfur electrode	=	t_{se}	
Thickness of sodium chamber	=	t_{Na}	

6.1 Total Mass of the Battery

The masses of sodium and graphite remain unchanged in terms of the mass of sulfur, therefore, as in the earlier cases:

$$\text{mass of sulfur per cell} = m$$

$$\text{mass of sodium per cell} = 0.476 m$$

$$\text{mass of carbon felt} = 0.0695 m$$

$$\text{Mass of electrolyte} = \frac{\pi D^2}{4} t \cdot 3.2 = 2.51 D^2 t$$

In order to calculate the mass of the cell wall, its dimensions should be known, t_{se} and t_{Na} should therefore be known.

$$\text{Volume of the cathode chamber} = 0.818 m.$$

$$\therefore t_{se} \frac{\pi D^2}{4} = 0.818 m$$

$$\text{or } t_{se} = 1.019 m/D^2$$

$$\text{Similarly } t_{Na} = 0.689 m/D^2$$

The overall length of the battery = $N[t_{se} + t_{Na} + t]$

Taking the assumed values of the cell bipole and end plate thickness and assuming stainless steel as the material. used, the total mass of the cell can be calculated as:

$$M = N[1.523 m + 2.51 D^2 t + 24.4 t_w(t_{se} D + t D + 0.689 m/D)] + 1.581 D^2 \quad (10)$$

Computation of t_{se} follows later.

6.2 Internal Resistance

The internal resistance per cell is:

$$R_{in} = \frac{t \rho_{\beta} + (t_{se} - 0.2) \rho_{se}}{\pi D^2 / 4}$$

because with $t_{se} < 2$ mm, the sulfur electrode shows negligible resistance¹².

Assuming

$$\rho_{\beta} = 5 \text{ ohm-cm}$$

$$\text{and } \rho_{se} = 10 \text{ ohm-cm}$$

at a working temperature of 300°C ,

$$\begin{aligned} R_{in} &= \frac{6.36}{D^2} [t + 2(t_{se} - 0.2)] \quad \text{when } t_{se} > 0.2 \\ &= \frac{6.36}{D^2} t \quad \text{when } t_{se} < 0.2 \quad (11) \end{aligned}$$

6.3 Specific Energy

For an N cell stack, the energy output W_o is given by:

$$\begin{aligned}
 W_0 &= m G N \left[1 - \frac{m G R_{in}}{E_{av}^2 T} \right] \\
 &= m G N \eta_d \quad (12)
 \end{aligned}$$

where m , R_{in} and E_{av} are per cell quantities.

Using eqns. (9)-(12), considering only positive sign in the solution of the quadratic equation,

$$t_{se} = 0.1 - t/4 + \frac{1}{4} \left[(t - 0.4)^2 + 1.376(1 - \eta_d) \frac{T E_{av}^2}{G} \right]^{\frac{1}{2}} \quad (13)$$

If eqn. (12) yields t_{se} less than 0.2, t_{se} is put equal to 0.2 in further computation. Using eqns. (3) and (10)-(13), the specific energy can now be computed with the variation of different dimensions and parameters. The performance is shown in figs. 3.8 and 3.9. The data used is listed below:

$$\begin{aligned}
 D &= 15 \text{ cm} \\
 t &= 0.2 \text{ cm} \\
 t_w &= 0.08 \text{ cm} \\
 T &= 1 \text{ hr} \\
 \eta_d &= 0.80.
 \end{aligned}$$

7. PRELIMINARY DESIGN OF A GENERAL PURPOSE VEHICLE BATTERY

7.1 General Requirements

The battery of a general purpose vehicle must be capable

of sustaining the car at 60 m.p.h. for about 200 miles and provide peak power to accelerate the car from rest to 60 m.p.h. in less than 13 seconds.^{1,2} This acceleration requirement requires about 90 kW from the battery. At 60 m.p.h. the traction motor would require about 20 kW. Therefore, the minimum requirements for a battery would be 20 kW and 20 kW-hr (for 60 miles range) and a peak power of 90 kW. Design considerations of the power processing and traction machinery suggest an O.C.V. of 240 V, and a minimum voltage of 150 V will provide a good compromise of light-weight motors and power processors and high system efficiency.

$$\text{Discharge time} = 20 \text{ kW-hr} / 20 \text{ kW} = 1 \text{ hr.}$$

$$I_{\text{peak}} = 90 \times 10^3 / 150 = 600 \text{ A}$$

$$\therefore \text{Resistance of the battery} = \frac{240 - 150}{600} = 0.150 \text{ ohm.}$$

Using this value of resistance and a power of 20 kW in the load, the battery voltage and current must be 225 V and 100 A respectively. Taking 400 mA/cm² as the operating current density, the required surface area per cell would be:

$$\frac{100}{.400} = 250 \text{ cm}^2.$$

$$\text{Number of cells required} = \frac{240}{2.016} = 120.$$

7.2 Masses of Reactants

The ideal energy density of a sodium-sulfur cell is 0.762 kW-hr/kg. In view of this, the ideal mass of

products

$$= \frac{20}{0.762} = 26 \text{ kg.}$$

$$\text{Mass of sulfur} = \frac{2.1}{3.1} \times 26 = 17.55 \text{ kg}$$

$$\text{Mass of sodium} = \frac{1}{3.1} \times 26 = 8.45 \text{ kg}$$

In practice, an energy density of about 200 W-hr/kg can be achieved, hence the overall mass of the battery would be about 100 kg.

7.3 Dissipation

The ohmic losses dissipated during cruising are:

$$(240 - 225)100 = 1.5 \text{ kW}$$

In addition to these losses, there is a TAS loss of about:

$$880 - 750 = 130 \text{ W-hr/kg of Na}_2\text{S}_3^{1a}$$

∴ Heat loss due to entropy change

$$= 130 \times 26 = 3.38 \text{ kW}$$

Therefore total heat to be dissipated = $1.5 + 3.38 = 4.9 \text{ kW}$

Hence the cooling system must dissipate about 5 kW at 300°C.

8. DISCUSSION

From the computed performance, the effect of the component dimensions on the specific energy can be seen to be quite large. The effect of discharge time and discharge efficiency is, however, more pronounced. But these are

governed by the application for which the battery has to be used. Therefore for a particular application, the component dimensions must be optimized. The electrolyte thickness is the most critical factor for a tubular cell, as shown by fig. 3.4.

Fig. 3.6 shows the performance as a function of tube diameter with number of tubes as a parameter (the curves are accurate only for large N , and $N = 1$). From these curves an optimum value of tube diameter can be found to be 1 cm for a single tube cell and ~ 0.75 cm for a 100 tube cell, under the conditions specified. The performance improves as the number of tubes per cell increase.

The sensitivity of the performance to tube length is very small beyond a length of about 10 cm as shown for a 100 tube cell in fig. 3.7.

In flat plate batteries, the performance improves with increase in the number of cell as expected (Fig. 3.8a). The specific energy is optimum at a discharge efficiency of ~ 0.8 for a 12 cell stack (Fig. 3.8b). With this efficiency of 0.8 as a fixed parameter and a discharge time of 1 hour, the performance of a 12 cell battery has been calculated, and is plotted in fig. 3.9. The electrolyte thickness is again found to be the most critical factor. A thickness of 0.2 cm has been taken as the datum because battery plates of large diameter and very small thickness are difficult to fabricate, and may break due to mechanical shocks.

In all the above mentioned computations, the electrolyte resistivity was taken as a constant. This was varied in the case of a single tube cell and the sensitivity of the performance to electrolyte resistivity is shown in Fig. 3.5 for two electrolyte thicknesses, one very small, 0.02 cm, and the other 0.1 cm. It is clear that as long as the variation is not very large (order of magnitude), the specific energy does not change much. In fact, the performance is more sensitive to electrolyte thickness rather than to electrolyte resistivity.

An electrolyte which has better mechanical properties and thus can be used in the form of very thin tubes or plates, need not have a very high conductivity in order to give good performance. Hence, for a candidate electrolyte material, the mechanical properties and electrical conductivity can be adjusted (by varying fabrication or composition) to optimize performance.

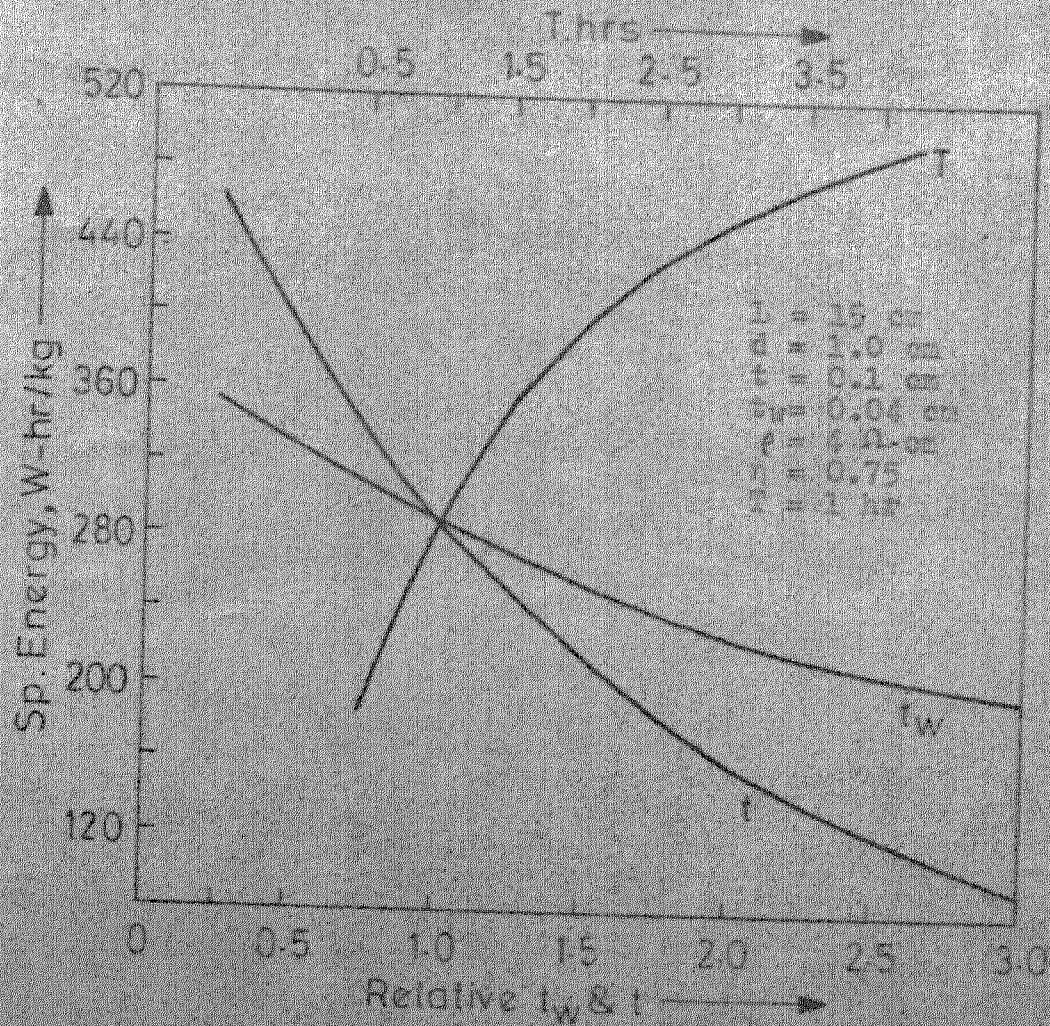


Fig. 3.4: Single tube cell — variation of specific energy with wall thickness, electrolyte thickness and discharged time

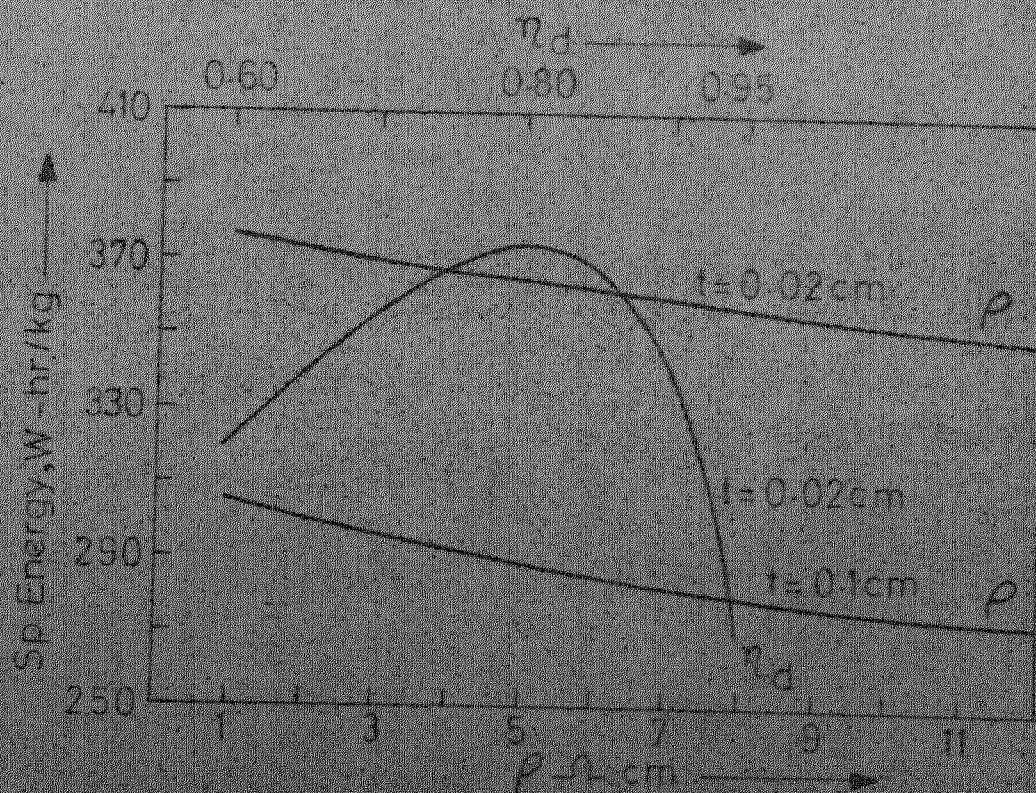


Fig. 3.5: Single tube cell — performance with variation in discharge efficiency and resistivity of electrolyte

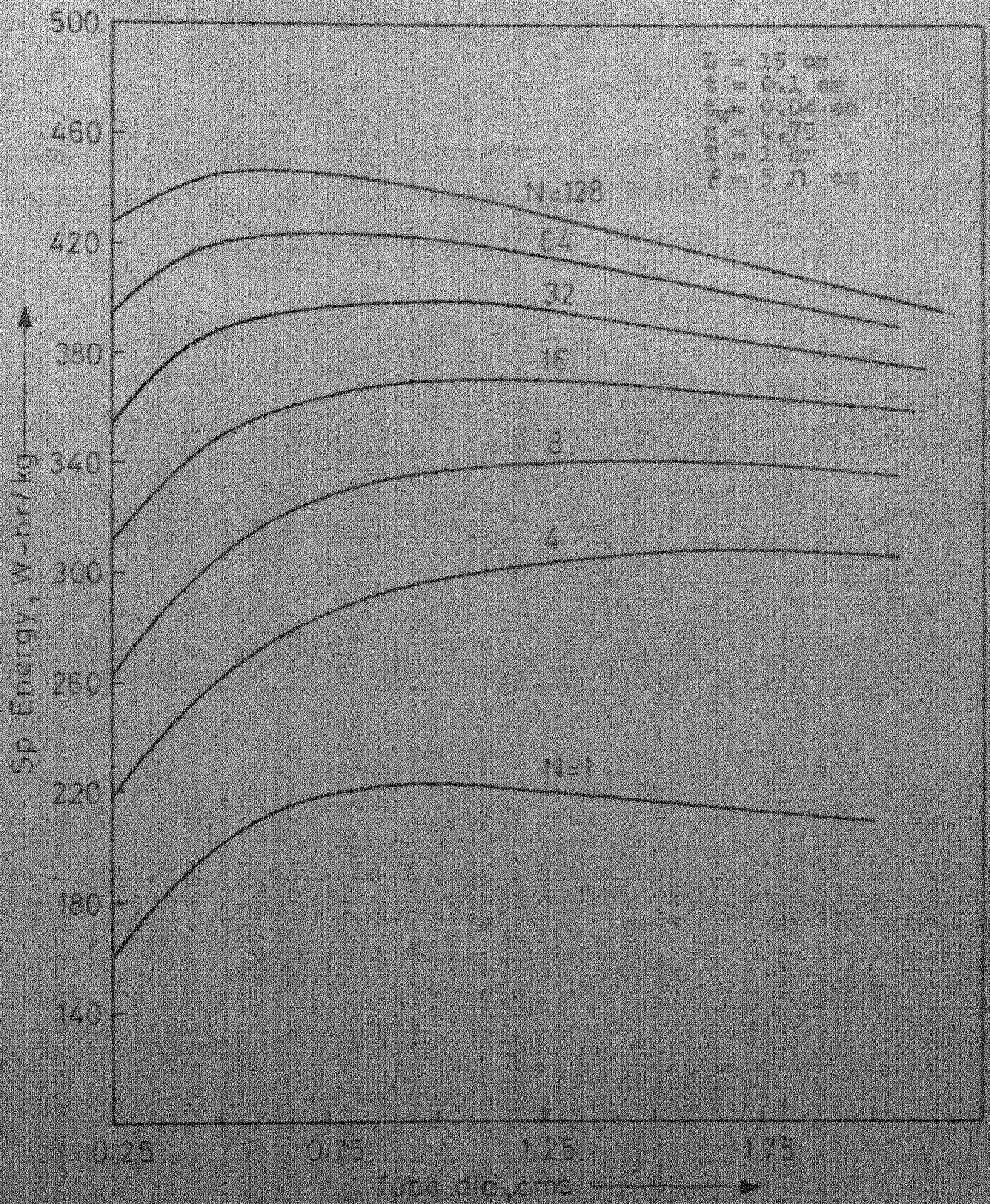


Fig. 3.6: Performance of a multitube cell with variation in diameter and number of tubes as a parameter

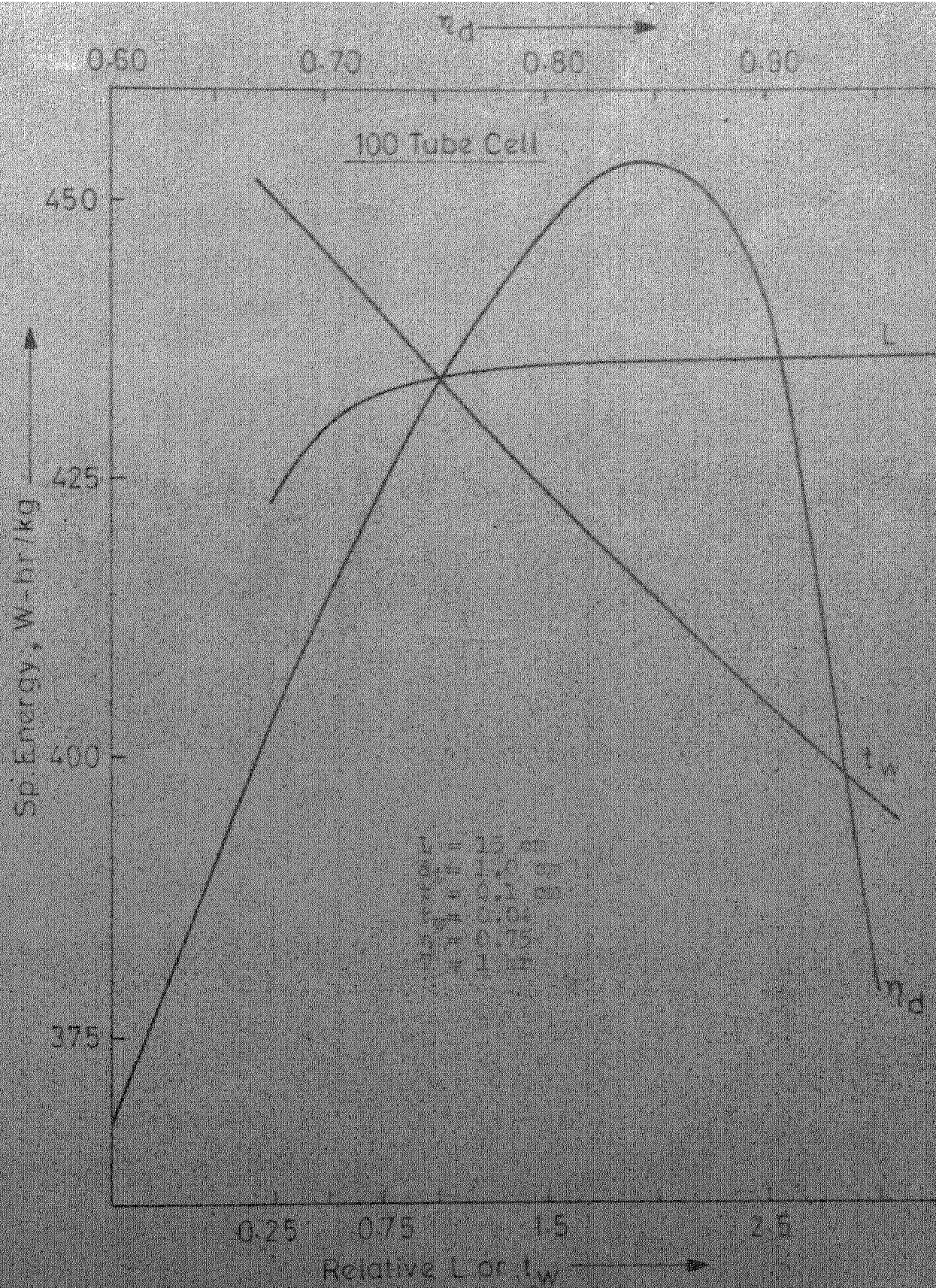


Fig. 3.7: Performance of a 100 tube cell with variation in discharge efficiency. Length of tube per cell wall is 15 cm.

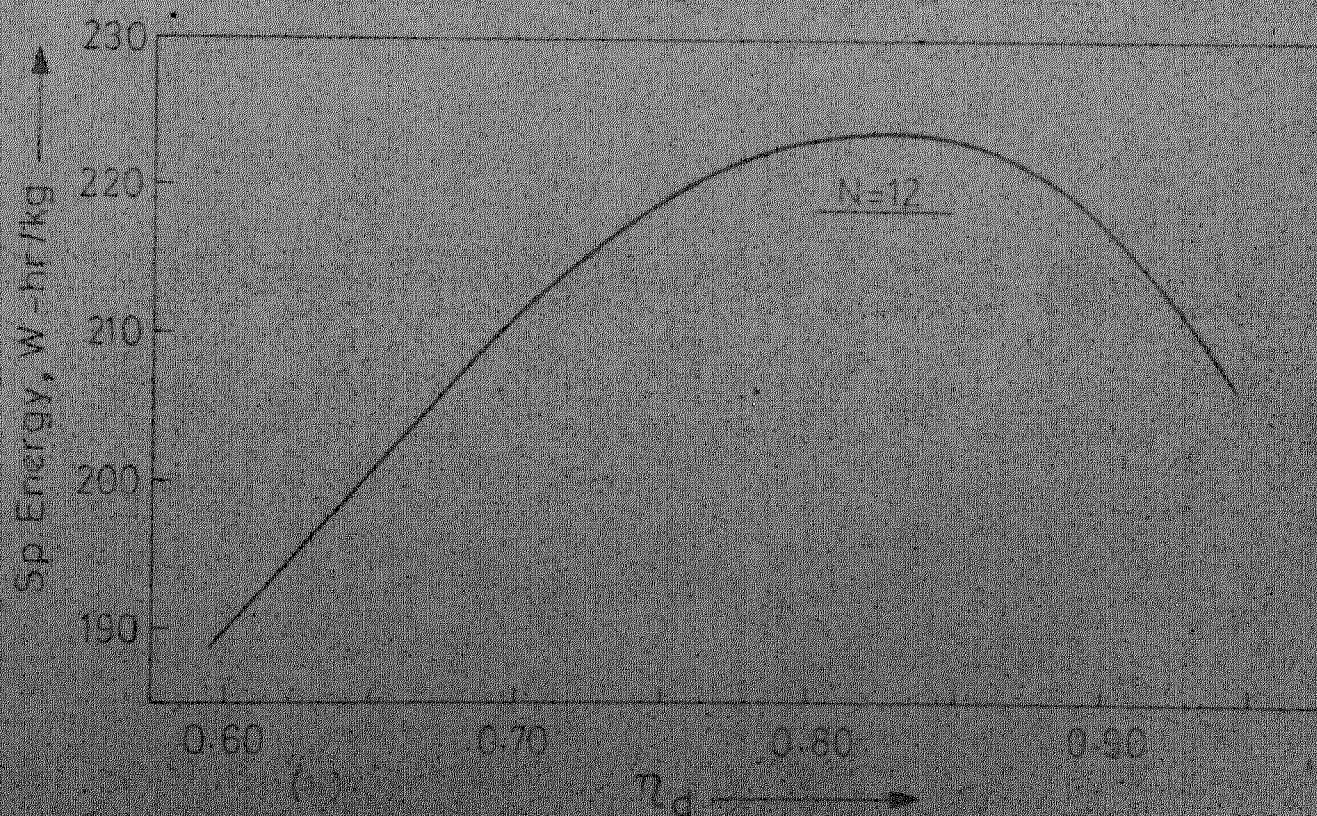
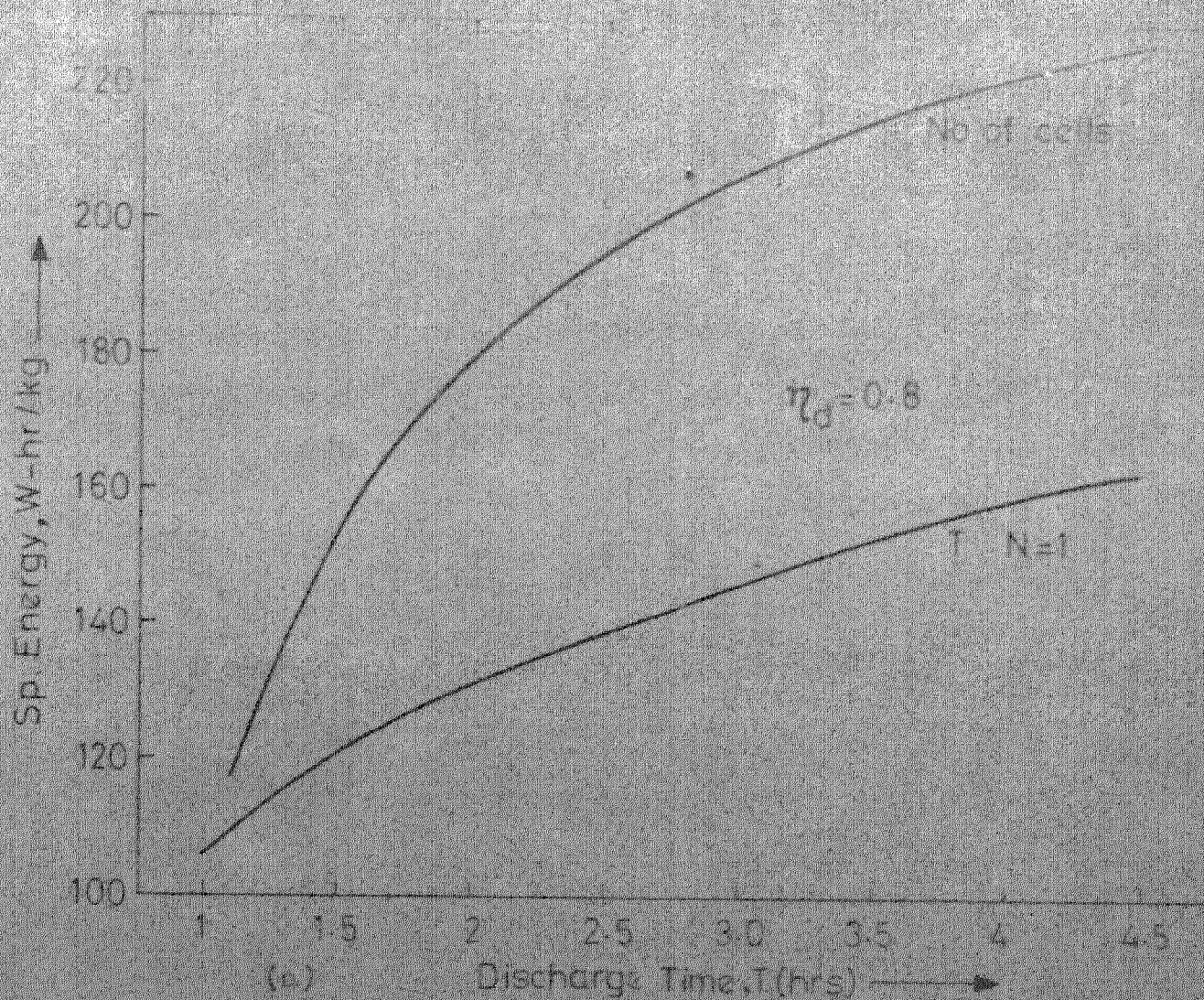


Fig. 3.8: Performance of a flat plate battery. Cell parameters: $V = 1.5$ V; $\eta_c = 0.7$ only; $\eta_e = 0.99$ only; $T = 1$ day; $n = 0.5$.

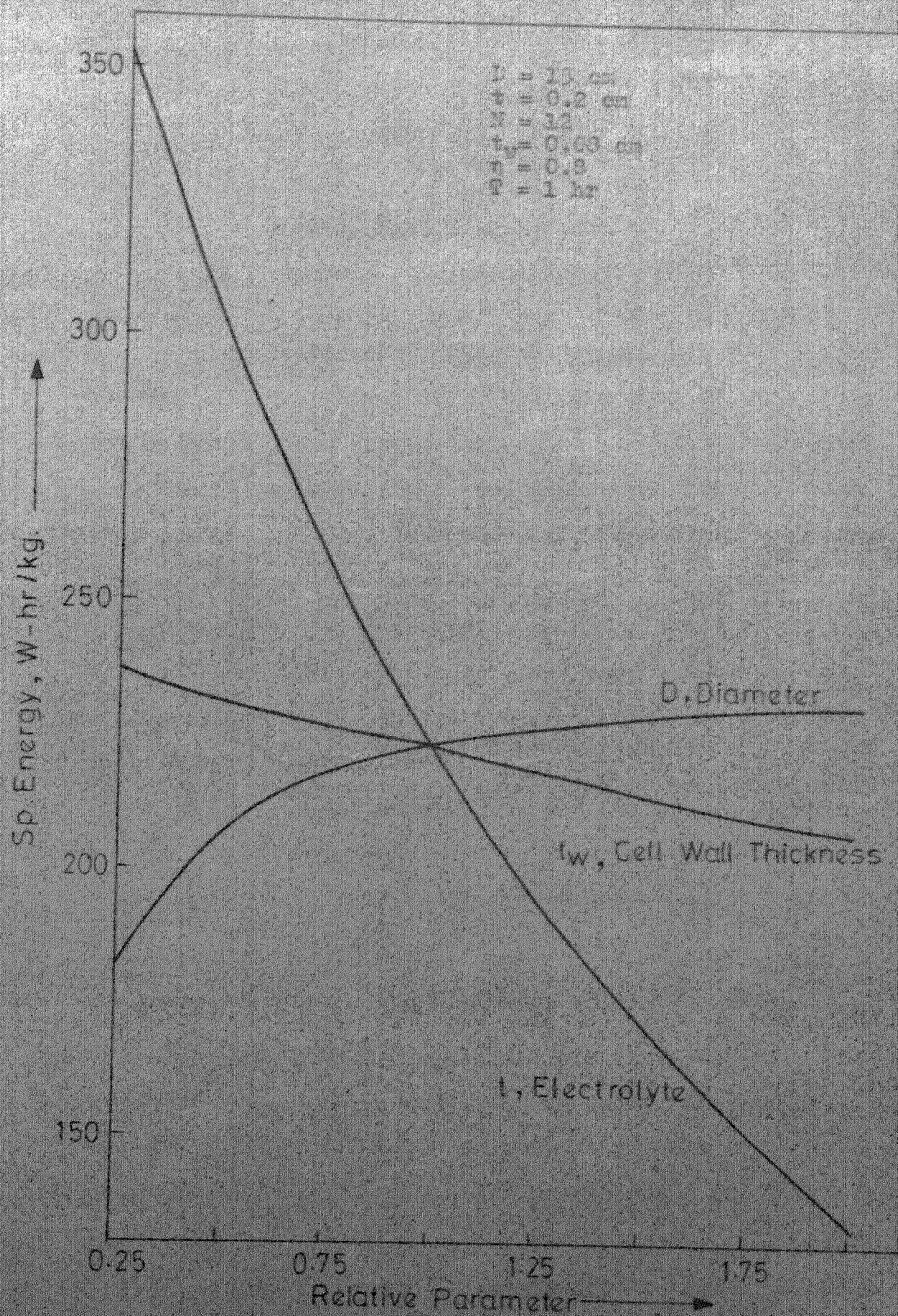


Fig. 3.9: Sensitivity of the specific energy of a 12-cell stack to cell diameter, cell wall thickness and electrolyte thickness.

CHAPTER IV

SOLID ELECTROLYTE MEMBRANE

1.1 General

The solid electrolyte membrane is the critical component of the sodium-sulfur cell, and most of the research has centred around developing it. The requirements of a membrane are stringent; good ionic conductivity, high electronic resistivity, impermeability, and reasonable life in use are essential properties.

Originally Ford Motor Co. examined glasses of the soda-alumina-silica system. No glass composition was found suitable and during investigation, a crystalline material beta-alumina was encountered. (Beta-alumina is not a form of Al_2O_3 but a sodium aluminate). The compound and its structure were known, but its high ionic conductivity had not been discovered. Beta-alumina was found to have the sought after properties.

1.2 Empirical Formula and Synthesis

β -alumina has the empirical formula $\text{Na}_2\text{O} \cdot 11\text{Al}_2\text{O}_3$ and when first named was thought to be an isomorph of Al_2O_3 , since the presence of soda was ignored or undetected. Later work proved the necessary presence of soda and the empirical formula mentioned above was a result of X-ray work. In reality, the compound is massively defective and contains a larger amount of soda than that indicated by the empirical

formula. Another compound designated β -alumina, with an empirical formula $\text{Na}_2\text{O} \cdot 5\text{Al}_2\text{O}_3$, also exists in the $\text{Na}_2\text{O}-\text{Al}_2\text{O}_3$ system.

β -alumina can be formed by heating Na_2CO_3 , with any one of the modifications of Al_2O_3 or its hydrates, to $\sim 1500^\circ\text{C}$. Heating to $\sim 1100^\circ\text{C}$ results in β'' -alumina, which converts to β -alumina and sodium aluminate at $> 1500^\circ\text{C}$. It is necessary to stabilize β'' -alumina to make it sinterable. This can be done by the addition of Li_2O or MgO . Above 1400°C , beta-alumina has an appreciable vapor pressure of Na_2O , which leads to its decomposition to α -alumina. Because of this, precaution must be taken in the synthesis of beta-alumina to prevent soda loss to the atmosphere. The Ford Motor Co. has used sealed platinum containers in which Na_2O atmosphere is maintained, to sinter Al_2O_3 - Na_2O - Li_2O compositions at a temperature around 1580°C , to get compositions nominally designated as β - Al_2O_3 Na_2O $6\text{Al}_2\text{O}_3$.²¹ Densities nearing the theoretical densities (3.25 gm/cc) have been achieved.

1.3 Crystal Structure

β -alumina has a hexagonal layer structure, with the lattice constants $a = 5.59 \text{ \AA}$ and $c = 22.53 \text{ \AA}$ (fig. 4.1). The Na ions are situated only in planes which contain, in loose packing, an equal number of Na and O ions (fig. 4.2). These planes are 11.27 \AA apart and are perpendicular to the c-axis. Between these sodium ion containing layers, there are four close-packed oxygen layers with appropriate Al ions

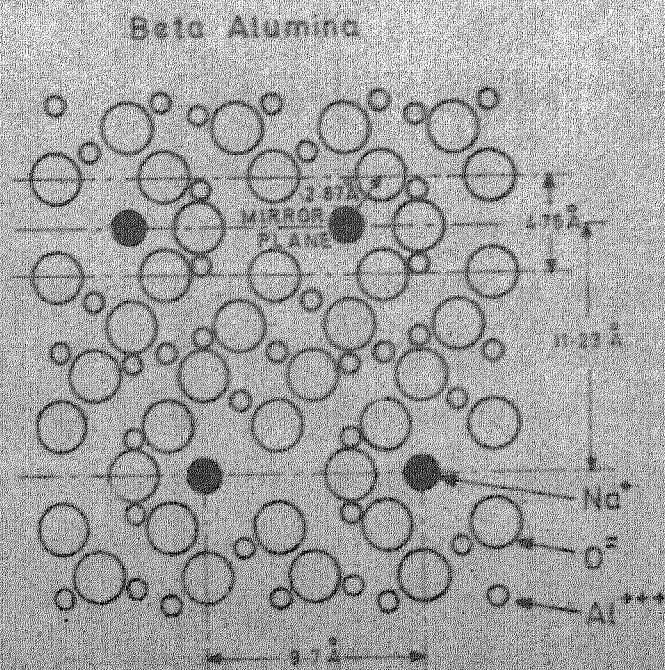


FIG 4.1 Arrangement of ions (110) plane of β -alumina crystal

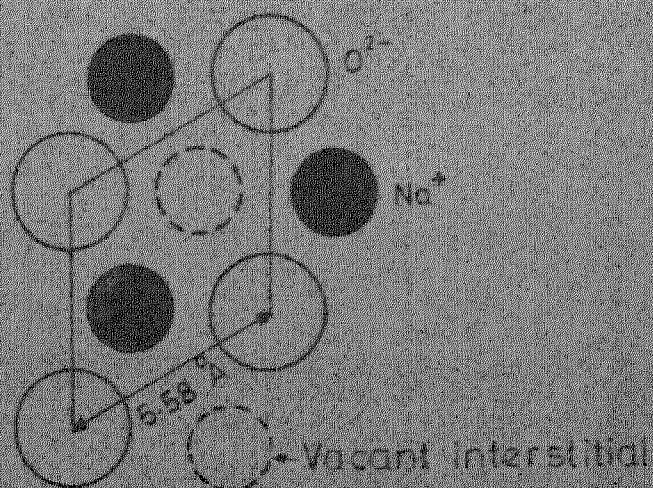


FIG 4.2 Arrangement of ions in the [NaO] layer

in both octahedral and tetrahedral holes. These close-packed blocks are sometimes referred to as 'spinel blocks' because of their similarity to spinel structure.

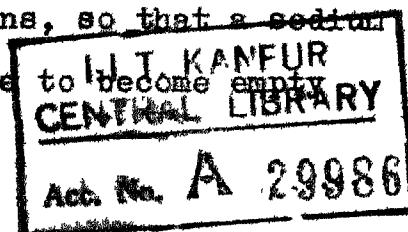
The spinel blocks above and below the Na ion containing layer are bound together not only by the sodium ions, but also by Al-O-Al bonds, giving rise to a rigid framework. Extra positions are available in the sodium containing layers for atoms in addition to the number given by the ideal empirical formula. The excess sodium ion concentration is probably neutralized by aluminum ion vacancies.

MgO stabilized β'' -alumina, having an idealized formula $\text{Na}_2\text{MgAl}_{10}\text{O}_{17}$ ($\text{Na}_2\text{O} \cdot \text{MgO} \cdot 5\text{Al}_2\text{O}_3$), and Li_2O stabilized β - Al_2O_3 $\text{Na}_2\text{O} \cdot 6\text{Al}_2\text{O}_3$ have rhombohedral structure that is very similar to the structure of hexagonal β -alumina, except that the c-axis is 1.5 times as large.

1.4 Ionic Conductivity

Consideration of the crystal structure of beta-alumina leads one to the conclusion that the diffusion of Na^+ ions in this material can occur two dimensionally, in a plane perpendicular to the c-axis, and a motion of the Na^+ ion in a direction parallel to the c-axis can not take place. This has been confirmed by experiments.⁶

The sodium ion containing planes are loosely packed, with sodium ions randomly distributed over sites, whose number is larger than the number of available ions, so that a sodium ion does not have to wait for another site to become empty.



before it can jump. The sodium ions are thus in a quasi-liquid state. The conduction is therefore a two-dimensional counterpart of the conduction exhibited by the other classes of 'super ionic conductors', viz. the alkali metal silver halides and defect stabilized ceramic oxides of the fluorite structure.^{24,25}

The variation of electrical conductivity with temperature for beta-alumina single crystal and polycrystalline phases is shown in fig. 4.3, on a log σ vs. $1/T$ plot. The higher conductivity of β'' -alumina may, in part, be due to difference in soda content between β'' and β -alumina, and the difference is the structure of Na^+ containing planes. The conductivity of the polycrystalline material is lower because the conduction is anisotropic and averaging takes place when crystallites are randomly oriented. Polycrystalline β'' -alumina has much larger conductivity than polycrystalline β -alumina and was therefore preferred for use as a solid-electrolyte in the sodium-sulfur cell. The electron transfer number of beta-alumina is nearly unity.^{7,30}

1.5 Ion-exchange Properties

The sodium ion in beta-alumina can be readily exchanged with numerous ions from molten salts.⁶ The monovalent ions that have been incorporated into the structure are: K^+ , Li^+ , Ag^+ , Rb^+ , NH_4^+ , NO^+ , Ga^+ , H_3O^+ , H^+ .

Na β -alumina has the highest ionic conductivity out of all these.

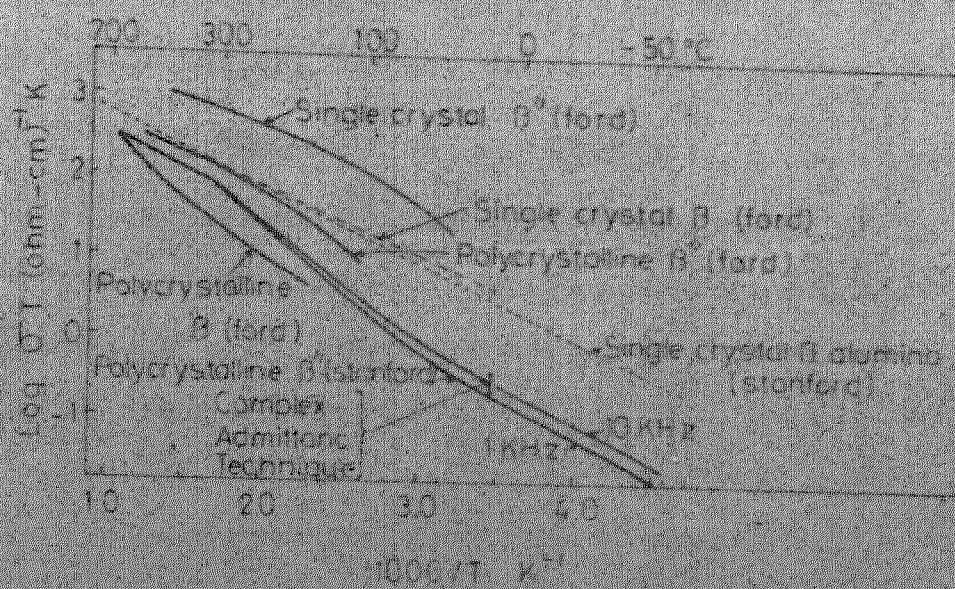


Fig. 4.3. Variation of electrical conductivity.

2. SCREENING OF THE ELECTROLYTE

The power and energy requirements of a sodium-sulfur battery critically depend on the ionic and electronic conductivities of the solid electrolyte. Prolonged electrolyte life requires resistance to crack formation during charging. Density, permeability, electron transport number and ionic conductivity tests, and mechanical strength tests after passage of current through it, are necessary for screening a material for the battery use.

2.1 Ionic Conductivity Measurement

The ionic conductivity of the highly conductive solids is very difficult to measure because of the problem of polarization at the electrodes. One way to avoid polarization is to use a reversible electrode, such as liquid sodium, for the measurement of d.c. Na^+ conductivity in beta-alumina. It is a common practice, however, to use a.c. at a frequency just large enough to avoid polarization, i.e. frequency at which the frequency dependence of conductivity disappears. With silver paste electrodes, a frequency in the MHz range is needed to avoid polarization in Na. β -alumina.

Different electrodes used are listed below*:

- i) Indium, at 500 KHz and 25°C, for single crystal^{6,30}
- ii) (a) Liquid sodium, at 1592Hz, 300°C, on sintered materials
- (b) Na/Hg amalgam

* See Table 6.6 for details.

- iii) (a) Ag paint²⁶
 - (b) evaporated Ag²⁸
- iv) Au (evaporated) 30-300°C
- v) Pt, at 800 KHz^{3c}
- vi) NaNO₃ (liquid) 320-400°C.²⁶
- vii) NaNO₃/NaNO₂ + Pt, 250-350°C.²⁶
- viii) Aqueous 5M NaNO₃, 30-80°C.²⁶
- ix) Tungsten bronze, d.c., -150°C-800°C.²⁷
- x) Evaporated aluminum contacts²⁹

High frequency of the order of 1 MHz is necessary with blocking electrodes. A lower frequency can be used with liquid electrodes. With tungsten bronze electrodes, which are both ionically and electronically conductive, and exhibit reversible behavior, a large temperature range can be covered without occurrence of polarization.

The electrode blocking problem has been solved by Mitoff³⁰ and Fally et al¹⁷, by the use of four probe method. This technique permits accurate determination of bulk conductivity when contact impedances approaching values as high as 10^{12} ohms are present. Low voltage a.c. current probes allow flow of current through the sample without providing a separate source of ions at the electrode. Low frequencies are preferred because high frequencies can capacitively by-pass grain boundary resistances. A frequency of 20 Hz (triangular waveform) was used by Mitoff with cathode sputtered Pt electrodes, and a frequency of 1 KHz

was used by Fally et al. with Pt or Ag paste electrodes.

An electrical screening procedure should be fast, simple and amenable to quick checking of a number of samples. The test should be accurate and require simple auxiliary equipment.

2.2 Study of Degradation

The life of the sodium-sulfur cell is almost invariably terminated by the failure of the solid electrolyte, due to crack formation during prolonged charging. It has been found that damage is initiated only ~~at~~ sites where sodium ions are converted to sodium atoms. At pre-existing surface cracks dendritic growth of sodium starts and advances into the electrolyte. The presence of metallic sodium has been confirmed by taking scanning electron micrographs of fractured surfaces¹², and a plausible mechanism of degradation has been suggested^{17,21}.

The molten sulfur and the sodium polysulfides have been found to have complete chemical compatibility with beta-alumina. Hence, for studying of the degradation of the electrolyte, the actual life determining conditions can be simulated in a NaNO_3 electrolysis cell or a Na/electrolyte/Na cell. From the sodium-sodium cell information regarding the interface properties can also be obtained.

CHAPTER V

EXPERIMENTAL PROCEDURE

1. FABRICATION OF MATERIAL

The detailed procedure for powder preparation, doping and sintering is given by Ray³². Identification of the resulting phases has also been carried out by him. Only a brief outline is included here for completeness.

1.1 Powder Preparation

(a) β -alumina: Na_2CO_3 (AR) and Al_2O_3 (Alcoa) were used as the starting materials for the preparation of β -alumina (as also for β^* -alumina). A eutectic composition of the two (36 mole % Na_2O 64 mole % Al_2O_3) was intimately mixed under extra pure acetone, and calcined at 1100°C for 4 hours. The reaction product was thoroughly mixed and subjected to an electric arc. For this, the powder was heaped on an alumina plate and enclosed by an alumina ring to prevent it from flying away. After fusing an appropriate amount, the torch was removed to allow the fused mass to solidify quickly. This fused mass was crushed, ground to a fine powder, then leached with dil. HCl , and washed to remove any NaAlO_2 formed. The resulting single phase β -alumina as determined by X-ray diffraction was dried and stored in a dry atmosphere.

(b) MgO Doped β -alumina: 2 wt. % MgO and 3 wt. % Na_2CO_3 were added to the β -alumina powder obtained by fusion and the mixture heated at 1200°C for 2 hours. The product was then

pelletized and heated at 1400°C for one hour in a platinum crucible. These pellets were later crushed, ground and leached to yield 1.25 wt. % MgO doped β -alumina.

(c) MgO Stabilized β'' -alumina: Al_2O_3 and Na_2CO_3 were mixed along with varying amounts of MgO and prereacted at 1100°C for 4 hours. The reaction product was homogenized under acetone and pelletized in a steel die at 5000 psi. The pellets were heated at 1350°C for 3 hours and then crushed, leached and ground to fine particle size. The resulting material was found to be stabilized β'' -alumina powder.

1.2 Pressing

The powders were ground to a finer size, under ethylene glycol, using a power-driven alumina mortar and pestle. After grinding for about 7 hours, ethylene glycol was removed by repeated washing and filtration. The powder was dried at 300°C for a few hours. The remaining ethylene glycol serves as a binder during pressing. Pressing was done using steel dies, and a hydraulic press. Discs of $1/4''$, $3/8''$ and $1''$ diameter, were pressed under pressures upto about 40,000 psi and then heated at 300°C for several hours to remove the organic matter.

1.3 Sintering

The sintering was carried out under coarse β -alumina powder, in alumina crucibles. The discs were presintered at 1400°C for 1 hour and then fired in a Zircoa pot furnace.

The temperature was maintained for 4 hours at 1700°C , (as measured by an optical pyrometer focussed on the top of the muffle that was used to cover the crucibles). The discs were taken out at about 150°C and transferred to a vacuum desiccator.

1.4 Density

Very little shrinkage occurred during sintering and the resulting fired densities are low compared to the theoretical density of β -alumina. The densities of the sintered specimens, for the various starting compositions are shown in Table 5.1.

Table 5.1
Fired Densities of Various Compositions

Symbol	Nominal Formula	wt. % Components			Fired density
		Na ₂ CO ₃	MgO	Al ₂ O ₃	
β''-alumina:					
A	1.13Na ₂ O.1.0MgO.5Al ₂ O ₃	17.88	6.02	76.1	2.55
B	1.13Na ₂ O.0.84MgO.5Al ₂ O ₃	18.05	5.15	76.8	2.50
C	1.13Na ₂ O.0.69MgO.5Al ₂ O ₃	18.22	4.25	73.29	2.40
β-alumina:					
D	pure β-alumina	36 (used for fusion)	-	64	2.8
E	1.25MgO.doped β-alumina	2% MgO added to D			2.4

2. CONDUCTIVITY MEASUREMENT

Two electrode systems were used to measure the conductivity of the beta-alumina specimens. (1) The silver paste system was used with 1/4" dia. pellets in the temperature range 200-350°C. (2) The molten NaNO_3 electrode system was used with 3/8" pellets in the temperature range 320-400°C. The discs were polished, first with diamond file and then with fine beta-alumina powder. The silver paste was applied in two successive thin layers, with baking at about 150°C for 2 hours, and was found to adhere satisfactorily. A quartz sample holder (fig. 5.1), was used for resistance measurements in air. Platinum leads were used to make contacts with the silver paste, using a spring-loaded alumina rod to press the flattened ends of the Pt wire against the Ag paste. The Pt leads were connected through a co-axial cable to the measuring bridge.

For the liquid electrode measurements with NaNO_3 , the beta-alumina discs were sealed to pyrex glass tubes, using 'Autostic' (Carleton Brown Ltd., England), an alumina-based cement, which does not react with the molten salt and has a negligible electrical conductivity. The cell used — shown in fig. 5.2 — was placed inside a temperature controlled electrical resistance furnace for measurement. Pt leads dipped in the melts were used as contacts. Small pads of carbon felt were put on either side of the disc. The Pt leads were connected through a very short coaxial cable to

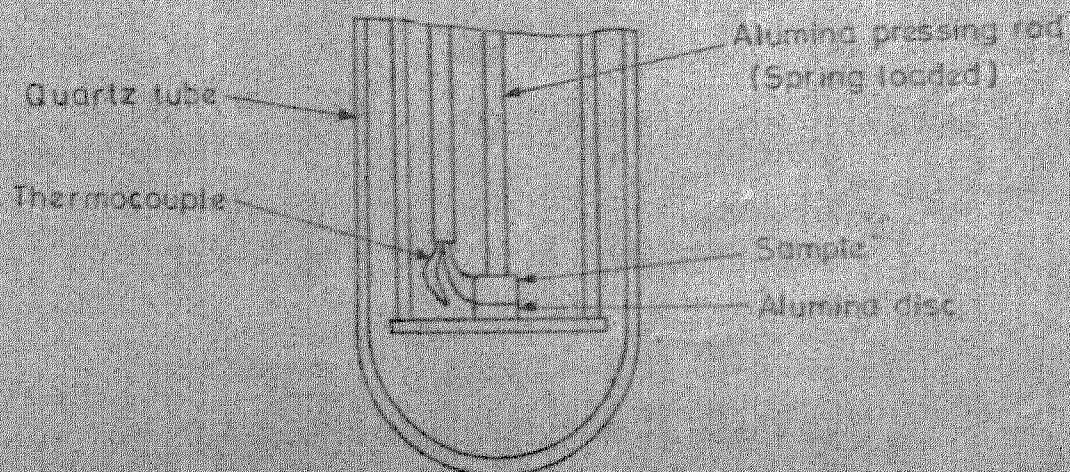


Fig. 5.14 Quartz sample holder for the silver paste meniscopets

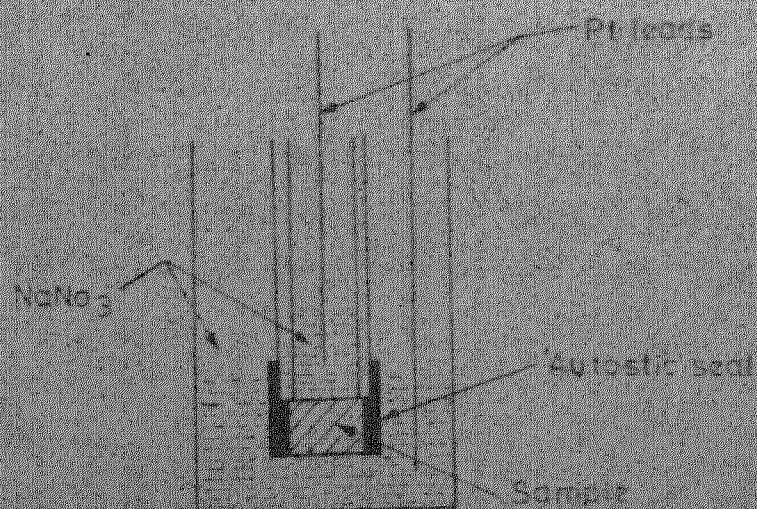


Fig. 5.20 Cell used for vertical conductivity measurement with liquid NaNO_3

the measuring bridge to reduce lead impedance.

General Radio 1606-A r.f. bridge was used together with a General Radio type 1211-C ~~unit~~ oscillator for resistance measurements at 1 MHz. BEL. RU 536 Cd receiver was used as the ~~de~~detector. This detector has a beat frequency oscillator that converts r.f. into a.f. The output was fed to a loud-speaker and a cathode ray oscilloscope in order to get a sharp null.

General Radio 1650 Bridge along with General Radio 1210-C R-C oscillator and type 1232-A tuned amplifier and detector was used to measure resistance at other audio frequencies (200 Hz to 20 KHz). The cells were placed inside a Kanthal heated furnace whose temperature was controlled within $\pm 0.5^{\circ}\text{C}$ by a Leeds and Northrup Electromax Controller.

Effort was made to keep the measuring chromel-alumel thermocouple as near to the sample as possible. Reproducibility of measurements was checked by making measurements both during heating and cooling.

3. SODIUM/SODIUM CELL

$3/8''$ discs of composition B (MgO stabilized β'' -alumina) and D (pure β -alumina) were used for these experiments. The discs were polished and sealed to a pyrex glass cell shown in fig. 5.3, using 'Autostic'. Both limbs of the cell had tungsten leads sealed to them. The assembly was checked for leaks under vacuum, upto 50 micron. Sodium metal, covered with liquid paraffin was transferred into both limbs of the

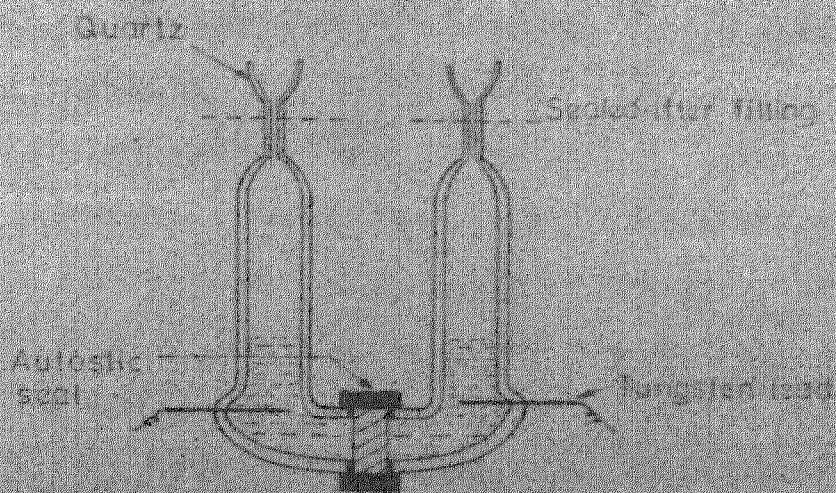


Fig. 5.3: Fe/Fe₂O₃/Fe cell schematic diagram

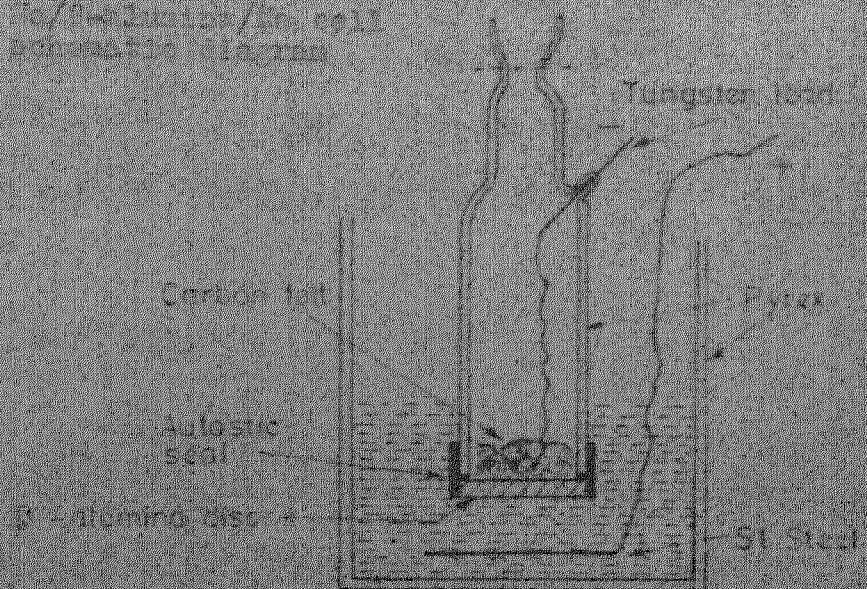


Fig. 5.4: Cell for electrolysis or electroplating

U-tube cells and then washed with benzene. Both limbs were immediately evacuated simultaneously and sealed after heating the cell to about 300°C using a heating tape. Since no attempt was made to purify the sodium before sealing, it should contain dissolved oxide.

The cell was placed in a temperature controlled electric furnace. Using a copper wire the leads were connected to the General Radio 1650 Impedance Bridge. Since liquid sodium does not readily wet the discs, a time lapse of about 6 hours at $\sim 375^{\circ}\text{C}$ was allowed for this. The 1 KHz resistance was taken at 1 hour intervals after the temperature reached $\sim 350^{\circ}\text{C}$. After the wetting took place, d.c. and 1 KHz resistances were measured in the temperature range $200\text{--}350^{\circ}\text{C}$. At two temperatures, viz., 350°C and 300°C , the resistance and series capacitance of the cell were measured as a function of frequency from 200 Hz to 20 KHz and at 1 MHz.

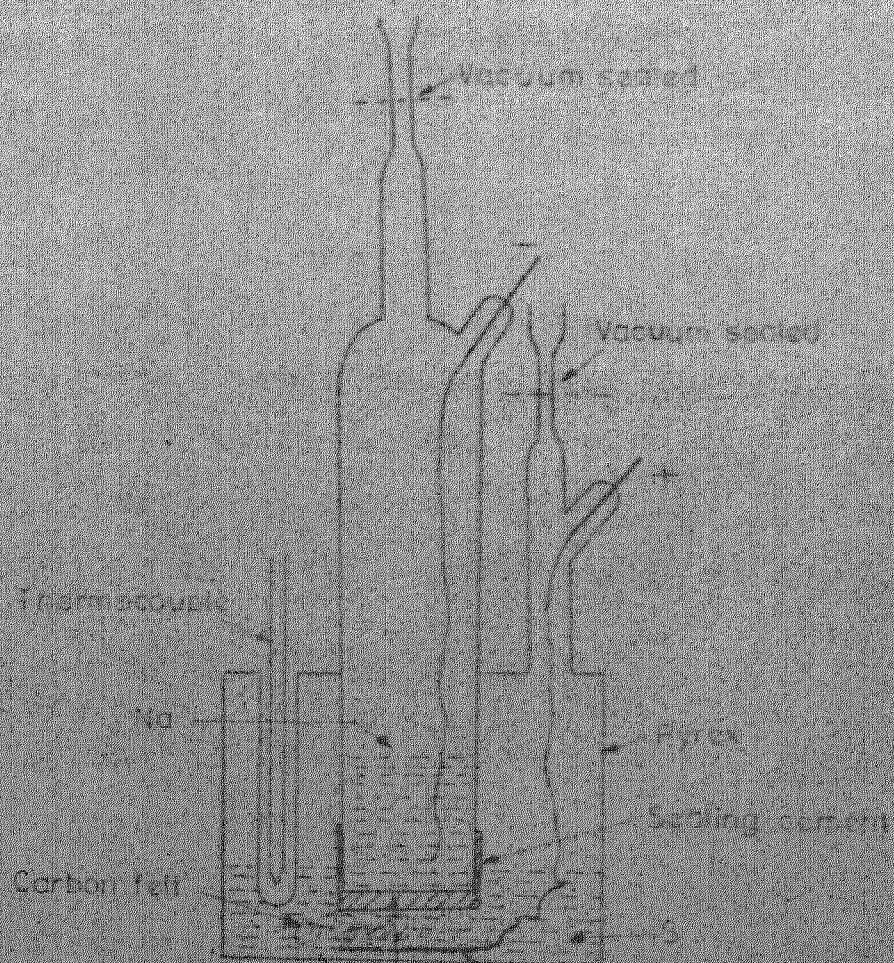
4. NaNO_3 ELECTROLYSIS

A 1 in. diameter polished disc was sealed to one end of a pyrex tube using 'Autostic'. A graphite felt pad was placed inside touching the disc, and a lead wire kept in contact with the felt. The tube was evacuated, filled with Argon at low pressure (1000 micron) and then sealed. This tube was dipped in a molten sodium nitrate bath at 320°C , held in another pyrex vessel in which a stainless steel electrode was dipped (fig. 5.4). Electric current was passed using the

NaNO_3 side as the cathode. A 6.3 V d.c. power supply in conjunction with a series resistance was used as a source. The voltage across the β -alumina sample was kept less than 3 volts, because electrolytic decomposition of β -alumina itself might occur otherwise. At first the carbon felt did not make a good contact and currents of only few milliamperes could be passed. After some time, the current increased gradually and was fixed at 20 mA by controlling the applied voltage. After passing a considerable charge through the cell the inner tube was weighed to check for any increase in mass. The total amount of charge passed was also noted. The tube was later broken and the disc examined to see any mechanical or visible degradation.

5. Na/S CELL

A 1 in. diameter disc of composition B was sealed to a pyrex glass tube by means of 'Autostic'. This tube was sealed to an outer glass vessel. Tungsten lead were sealed to both compartments using glass to metal seals (fig. 5.5). The cell was filled with 4 gms of Na and 10 gms of sulfur, sealed and tested for the e.m.f. developed.



St. Steel current collector
Solid-sodium electrolyte

Fig. 1. Schematic diagram of the vacuum-sealed cell for the study of the reaction of sodium with carbon felt.

CHAPTER VI

RESULTS AND DISCUSSION

Proper electrical characterization of a solid electrolyte can be carried out only on a dense ceramic, preferably composed of a single phase. As shown in Table 5.1, the present samples have densities ranging from 2.4 to 2.8 gms/cc, compared to a theoretical density of about 3.2 gms/cc. In addition to this relatively low density, these samples were found to contain phases other than β and β'' alumina.³² These factors should be expected to affect their electrical behavior and should therefore be kept in mind in the analysis of the electrical data.

1. CONDUCTIVITY MEASUREMENT—RESULTS1.1 Silver Paint Electrodes

Resistance measurements at 1 MHz, in the temperature range 200 - 350°C, were carried out with the five sample compositions. A through E, using silver paint electrodes. The results tabulated in Table 6.1, have been plotted in Fig. 6.1 as a $\log \sigma$ vs. $1/T$ plot. Using the Arrhenius relation

$$\sigma_T = \sigma_0 \exp(-E/RT)$$

where σ_T = electrical conductivity at temperature T,

σ_0 = pre-exponential factor,

and E = activation energy,

the activation energies (E) have been calculated from the slopes of the plot and have been included in table 6.1.

Table 6.1
Conductivity Data with Silver Paste Electrodes

$$f = 1 \text{ MHz}$$

Sample	Specific conductivity σ , $10^{-3} (\text{ohm-cm})^{-1}$							Activation energy kJ/mole
	Temp. °C	200	225	250	275	300	325 350	
A		8.0	8.5	9.4	11.4	13.3	16.0 17.7	17.0
B		3.2	4.6	5.4	6.5	8.0	9.0 10.9	19.2
C		2.8	3.6	4.1	4.8	5.7	6.4 6.5	15.9
D		1.3	1.5	1.7	2.1	2.4	2.6 3.5	14.5
E		1.7	2.1	2.6	3.1	3.2	3.7 4.5	15.8

Table 6.2
Conductivity Data for NaNO_3 Electrodes

$$f = 1 \text{ MHz}$$

Sample	Specific conductivity σ , $10^{-3} (\text{ohm-cm})^{-1}$						Activation energy kJ/mole
	Temp. °C	320	340	350	360	380 400	
A		65.1	75.0	79.0	85	90 100	16.5
B		60	70	73	75	78 80	14.0
C		58	61	64.7	65.5	70 73	13.5
D		28	31.4	32	33.5	34 36.6	13.0
E		72.7	78	80	82.7	85.7 86	15.5

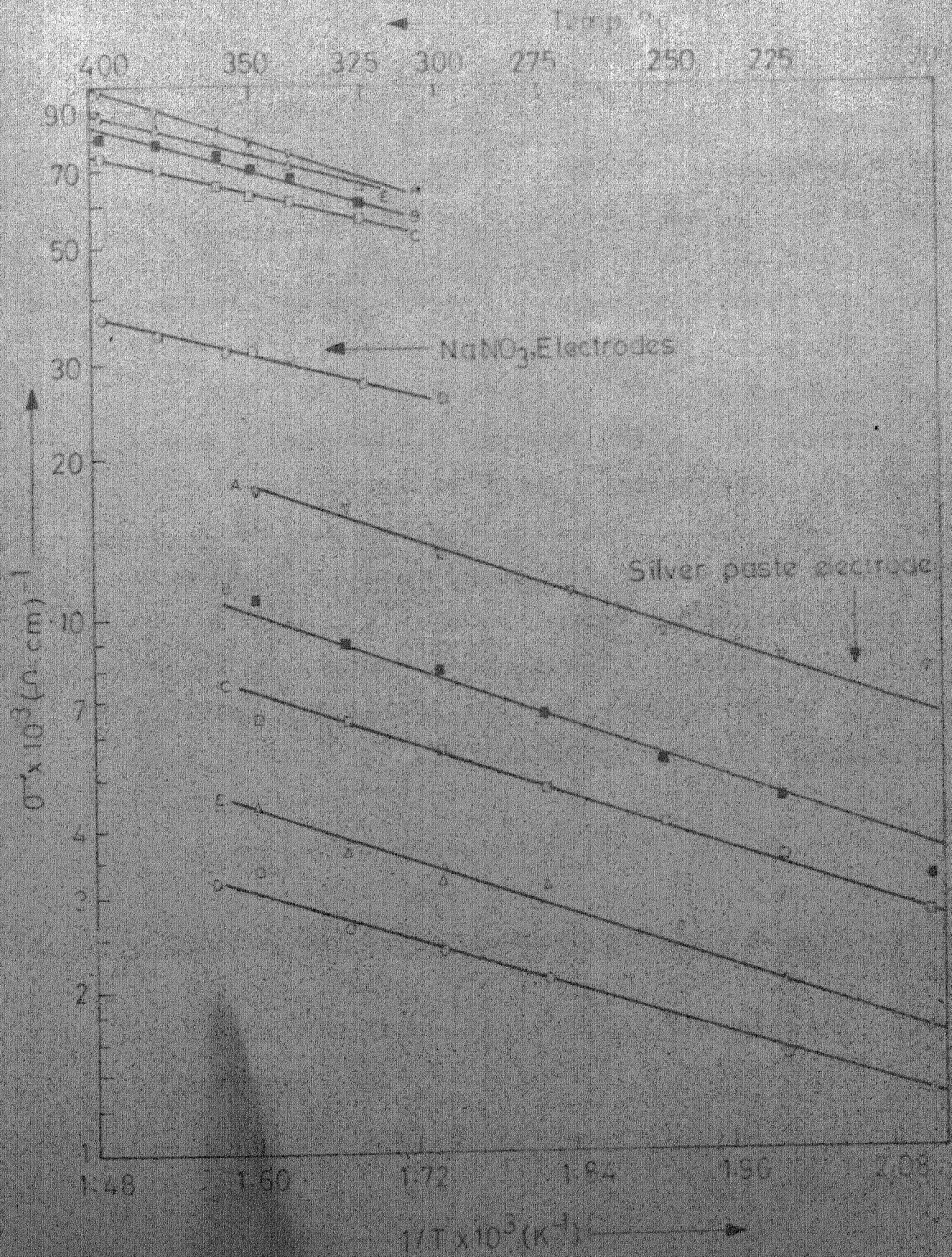


Fig. 2. Temperature dependence of the conductivity for silver paste electrodes (A-F) and NaNO_3 electrodes (O). The conductivity was measured at a frequency of 100 Hz.

1.2 NaNO₃ Liquid Electrodes

Molten NaNO₃ electrodes were used for measurement of resistance with frequency in the range 200 Hz to 20 kHz and also at 1 MHz at 350°C and 400°C (Table 6.3 and Fig. 6.2). In the measured frequency range, the conductivity increases more steeply in the lower frequency range than at high frequencies. In the case of sample D, the conductivity attains a constant value at 10 kHz or less where as for other samples, the conductivity increases slowly even beyond this frequency. This indicates that, polarization effects are generally important at frequencies below about 10 kHz and become small or absent at frequencies of about 1 MHz. As a practical measure, the conductivities of all the samples were measured at 1 MHz in the temperature range 320 - 400°C (Table 6.2, Fig. 6.1). The activation energies calculated from log σ vs. $1/T$ plots (Fig. 6.1) are included in Table 6.2.

The effective diameter of the pyrex tube was taken as the effective diameter of the sample. The resistance of the cell arrangement with an insulating cement layer on the sample, was found to be about 50 kilo-ohm compared to the average sample resistance of about 20 ohms, and therefore the error introduced was neglected.

1.3 Liquid Sodium Electrodes

The resistance of the sodium/ β -alumina/sodium cell is a function of the wetting of the ceramic by liquid sodium, which is a function of time and temperature. The resistance variation

Table 6.3
Variation of Conductivity with Frequency
Molten NaNO_3 Electrodes

Sample	Conductivity σ , $10^{-3} (\text{ohm-cm})^{-1}$							
	frequency KHz \rightarrow	0.2	1	2	5	10	20	1000
I) Temp. = 350°C								
A	20	43.1	52.6	58.5	65.0	70.0	79.1	
B	-	38.6	47.0	52.0	58.0	60.0	73.2	
C	-	37.5	43.0	46.0	50.0	55.0	64.7	
D	-	26.0	27.0	30.0	31.0	31.4	31.5	
E	-	40.7	52.2	63.2	78.9	79.0	80.0	
II) Temp. = 400°C								
A	35	58.3	64.2	79.0	80.0	87.0	100.0	
B	-	47.0	55.0	60.0	65.0	70.0	80.0	
C	-	44.0	50.0	55.0	60.0	65.0	73.0	
D	20	30.1	31.2	32.8	33.0	34.2	36.0	
E	-	48.6	57.5	64.0	72.0	74.5	86.0	

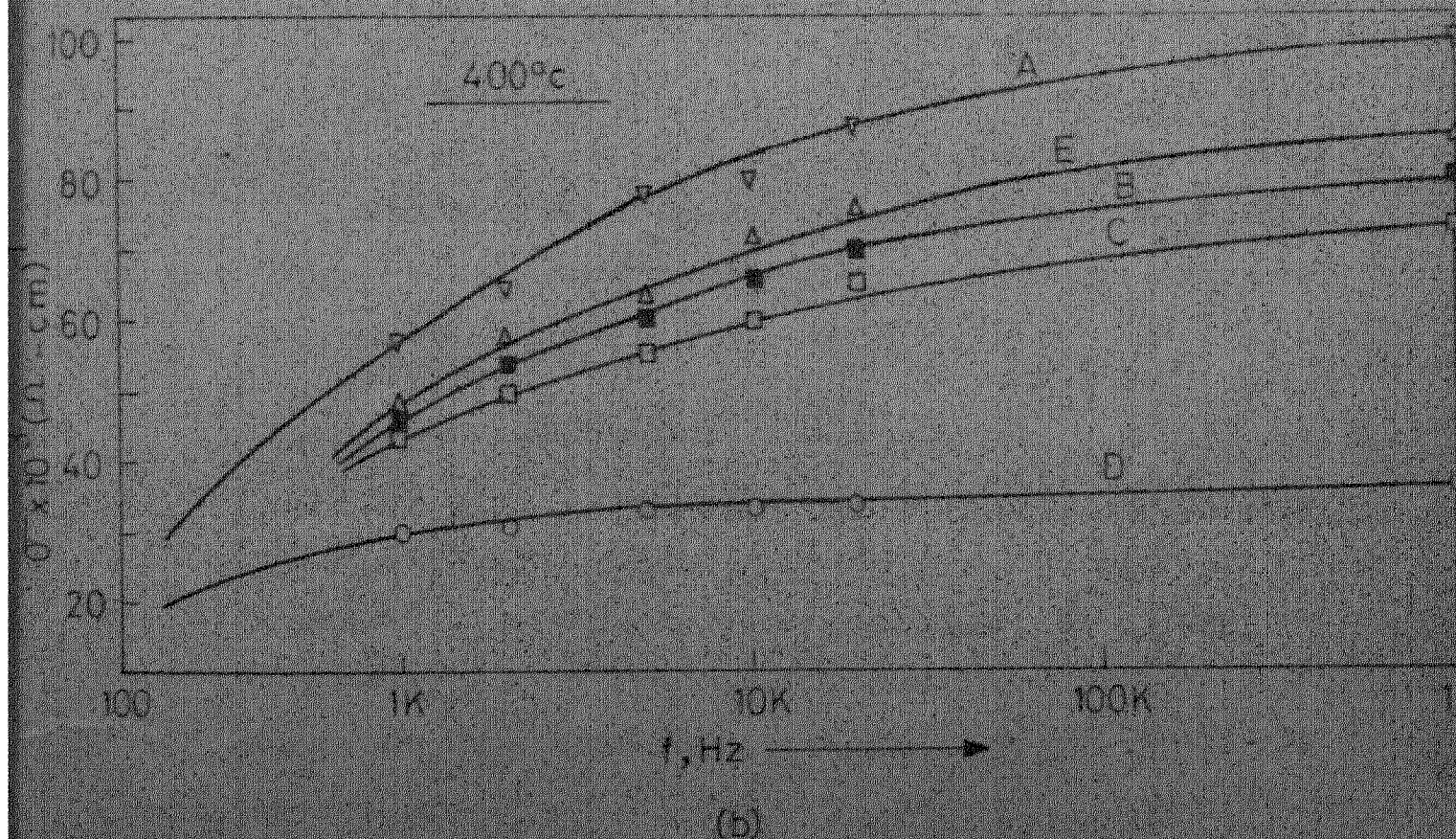
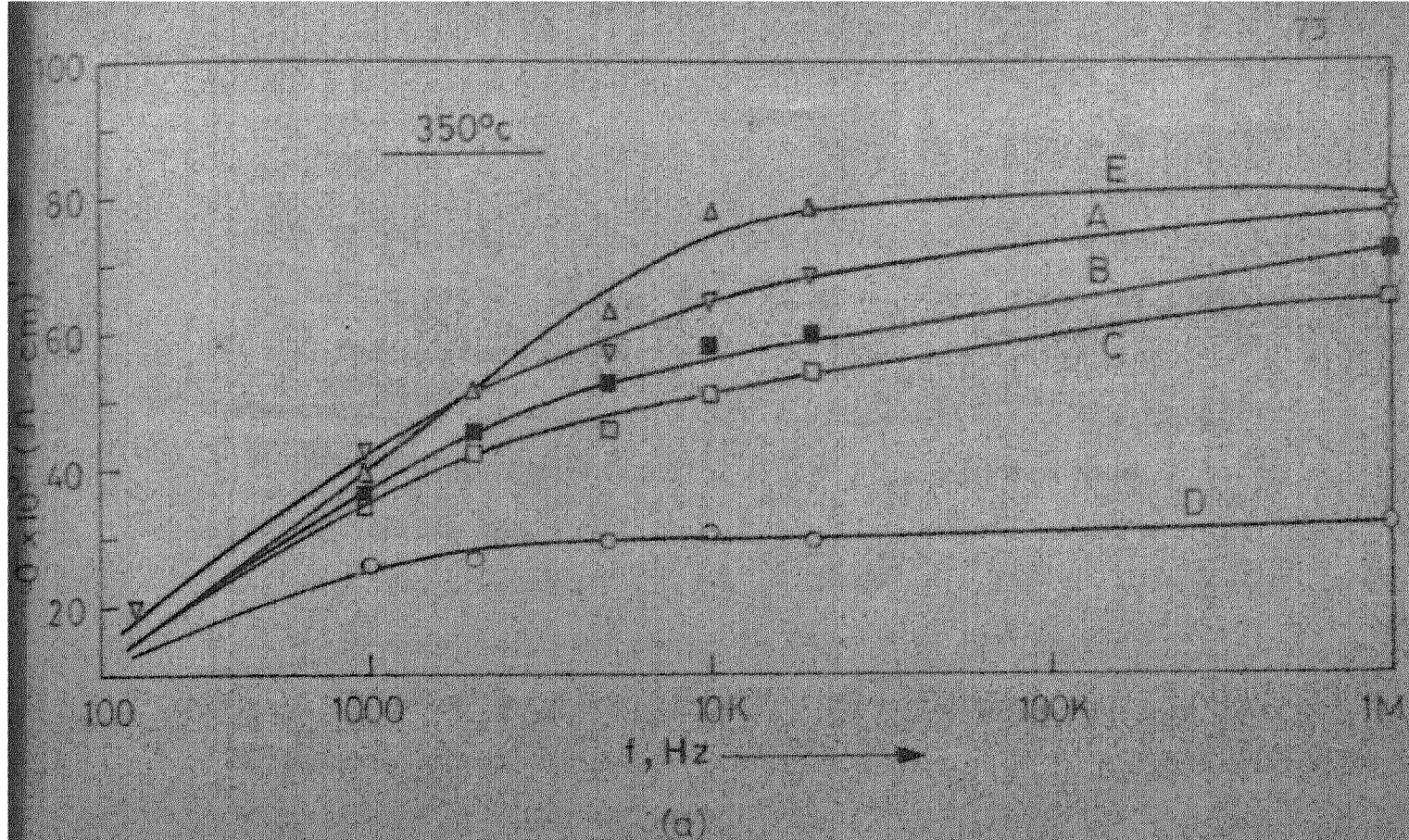


Fig. 0.2: Variation of conductivity with frequency (a) at 350°C, (b) at 400°C with silver NaNO_3 electrodes

of a β'' -alumina (composition B) sample is shown in Fig. 6.3, as a function of time. The resistance was measured at 1 kHz at a temperature of about 375°C. The conductivity vs. temperature for a pure β -alumina sample (D) in the range 200-350°C measured at a frequency of 1 kHz and with d.c. is tabulated in Table 6.4 and plotted in Fig. 6.4. The variation of resistance with frequency at 300°C and 350°C for pure β -alumina sample (D) is shown in Fig. 6.5 and Table 6.5.

Series capacitance of the pure β -alumina sample was measured at 300°C and 350°C with frequency as a parameter. The corresponding reactance values were calculated and plotted along with resistance values on an impedance plane to yield Cole-Cole type diagrams (Fig. 6.6). The diagrams have been completed on the low frequency side by joining the value at the lowest measured frequency with the value at d.c. This was done since measurements could not be carried out at very low frequencies.

2. DISCUSSION OF CONDUCTIVITY RESULTS

The results obtained with silver paste, molten sodium nitrate and liquid sodium electrodes are discussed here in terms of (i) electrode systems, (ii) composition, (iii) temperature and (iv) frequency of measurement. The liquid sodium electrodes were used only with a pure β -alumina sample (D), to measure impedance as a function of frequency and temperature. The results thus obtained will be discussed in detail under a separate heading.

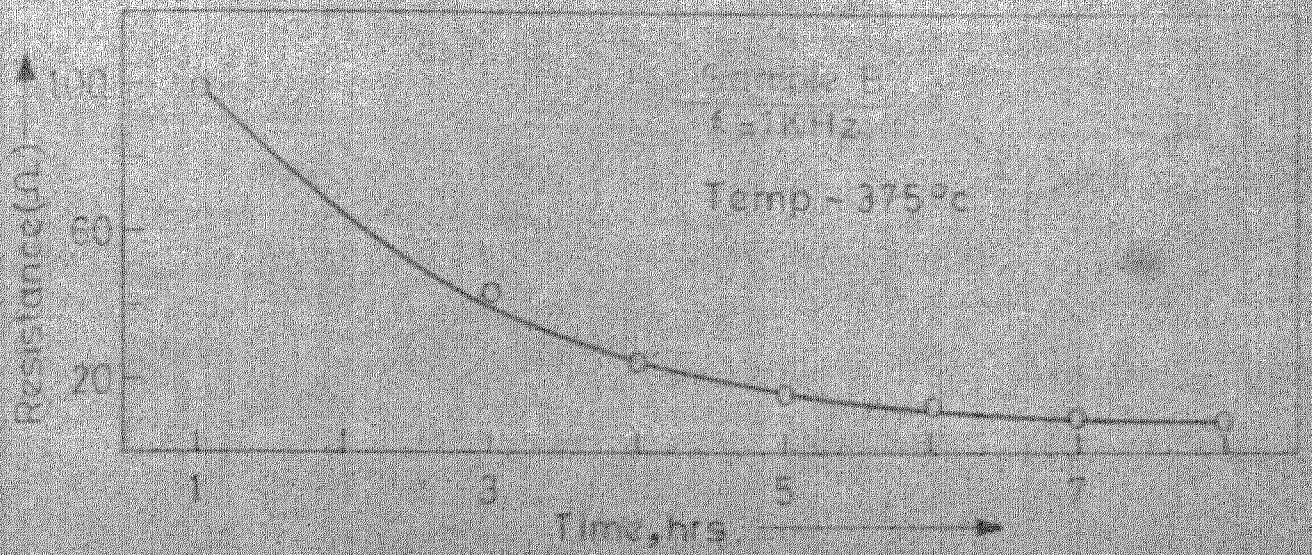


Fig. 5.27: Variation of the resistance of a $\text{Ba/Pb} - \text{BaTiO}_3$ ceramic with time

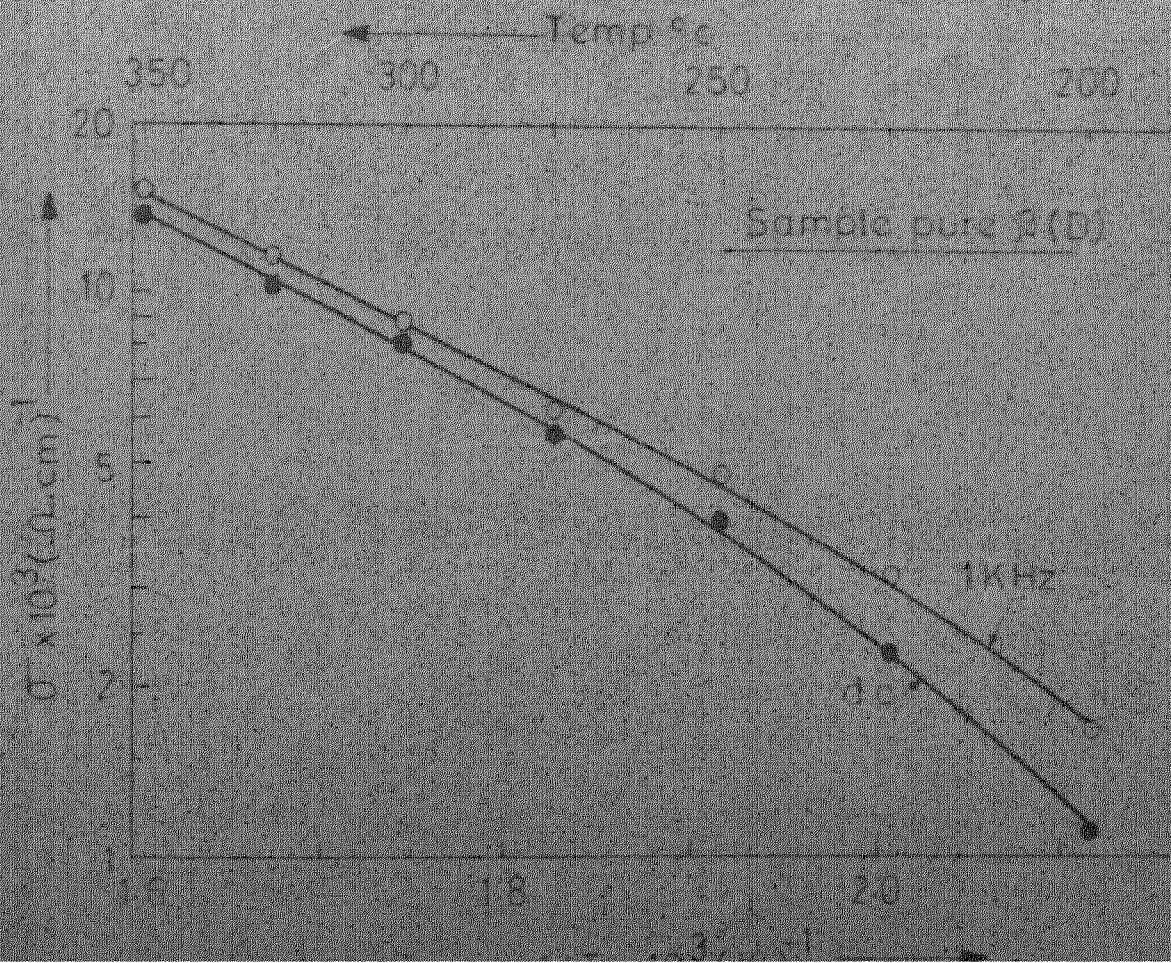


Table 6.4
Resistance
Variation of Na/ β -alumina/Na Cell with Temperature

Temp. °C	200	225	250	275	300	325	350
----------	-----	-----	-----	-----	-----	-----	-----

I) $f = 1 \text{ KHz}$

R, ohms	85.4	60.2	40.5	30.8	21.2	16.5	12.6
$\sigma \times 10^3, (\text{ohm-cm})^{-1}$	2.24	3.17	4.72	6.20	8.75	11.60	15.16

II) D.C.

R, ohms	100	75	45	34	23	18.5	13.8
$\sigma \times 10^3, (\text{ohm-cm})^{-1}$	1.91	2.54	4.25	5.62	8.30	10.12	13.8

Table 6.5
Na-electrode Impedance Data with
Frequency as a Parameter

I) Temp. = 300°C

f, Hz	d.c.	200	500	1k	2k	5k	10k	20k	1M
R, Ohms	23.0	21.6	21.3	20.8	20.5	20.4	20.2	20.15	20.0
C _s , μF	-	1.3	1.2	1.1	1.08	0.98	0.90	0.8	-
1/wC _s , ohms	-	612.3	265.3	134.9	72.3	32.5	17.7	10.0	-

II) Temp. = 350°C

R, Ohms	13.8	13.0	12.8	12.6	12.5	12.4	12.35	12.32	12.30
C _s , μF	-	4.0	2.4	1.3	1.1	1.08	1.05	1.05	-
1/wC _s , ohms	-	199.0	132.7	132.5	72.4	29.5	15.2	7.5	-

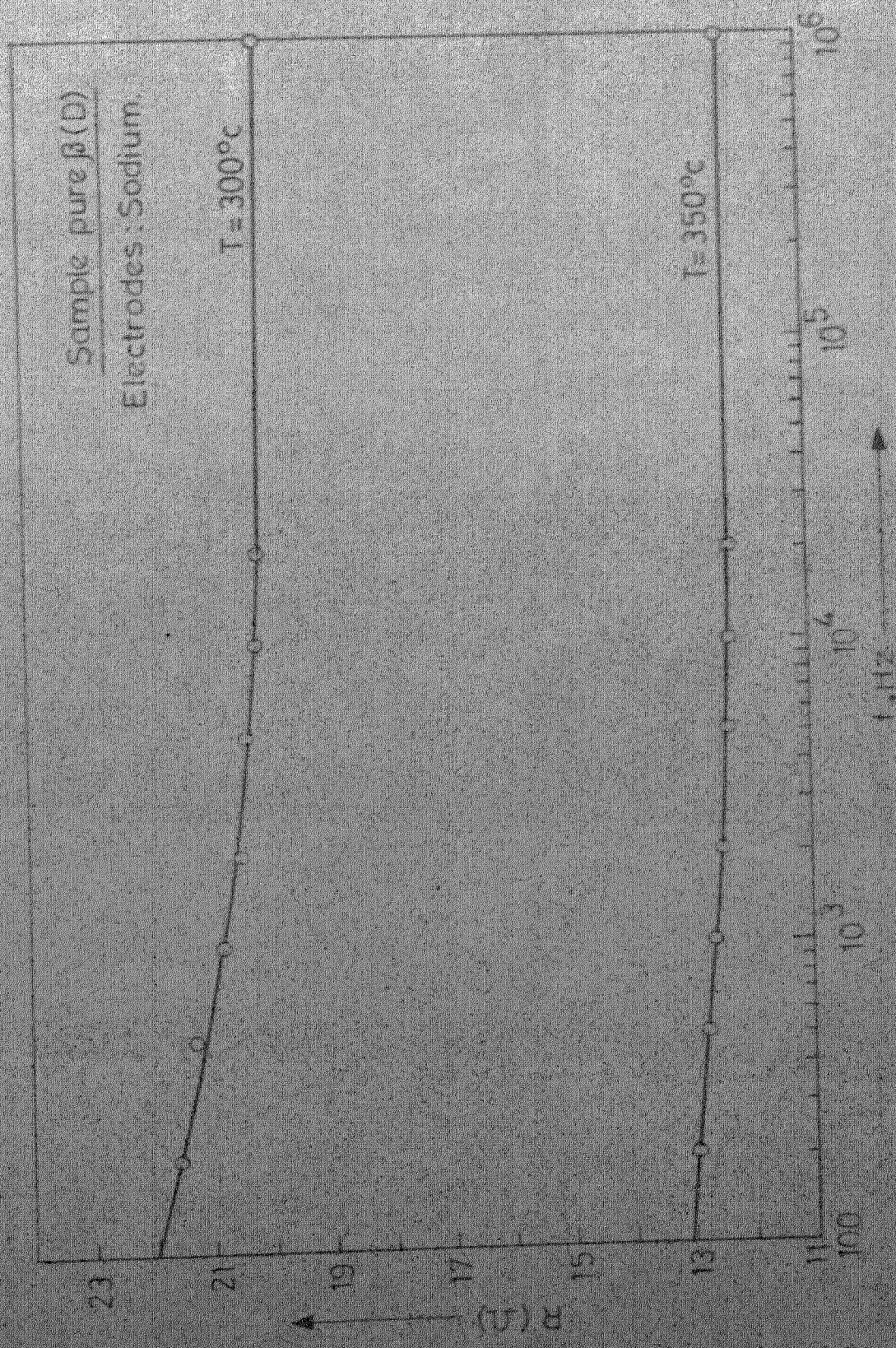
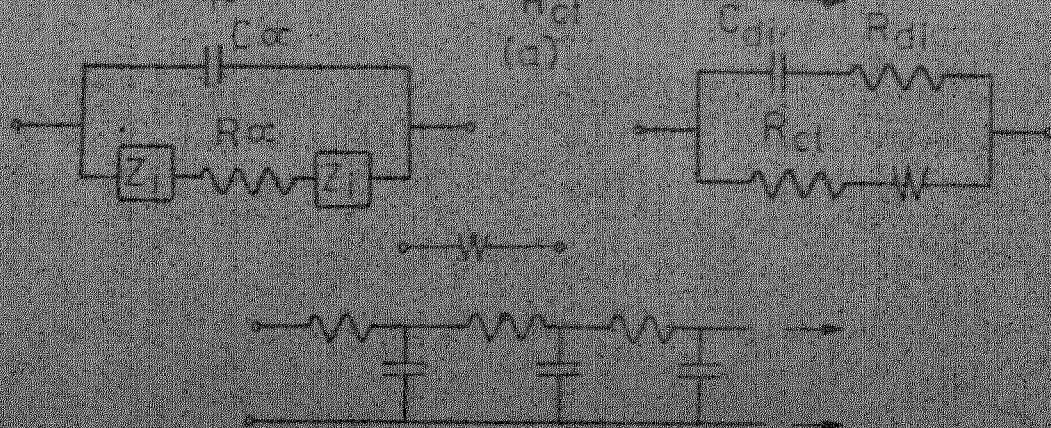
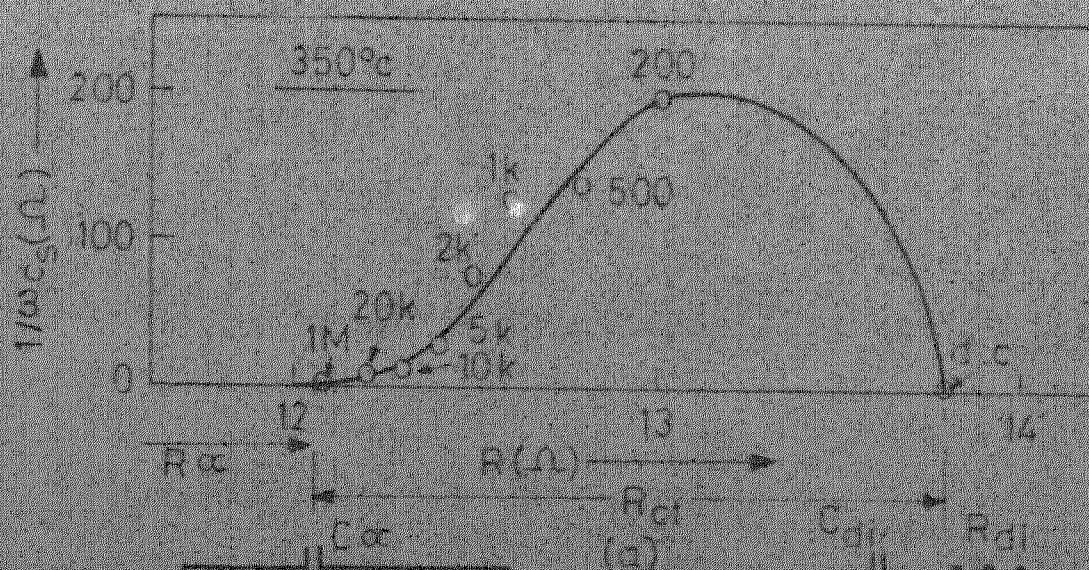
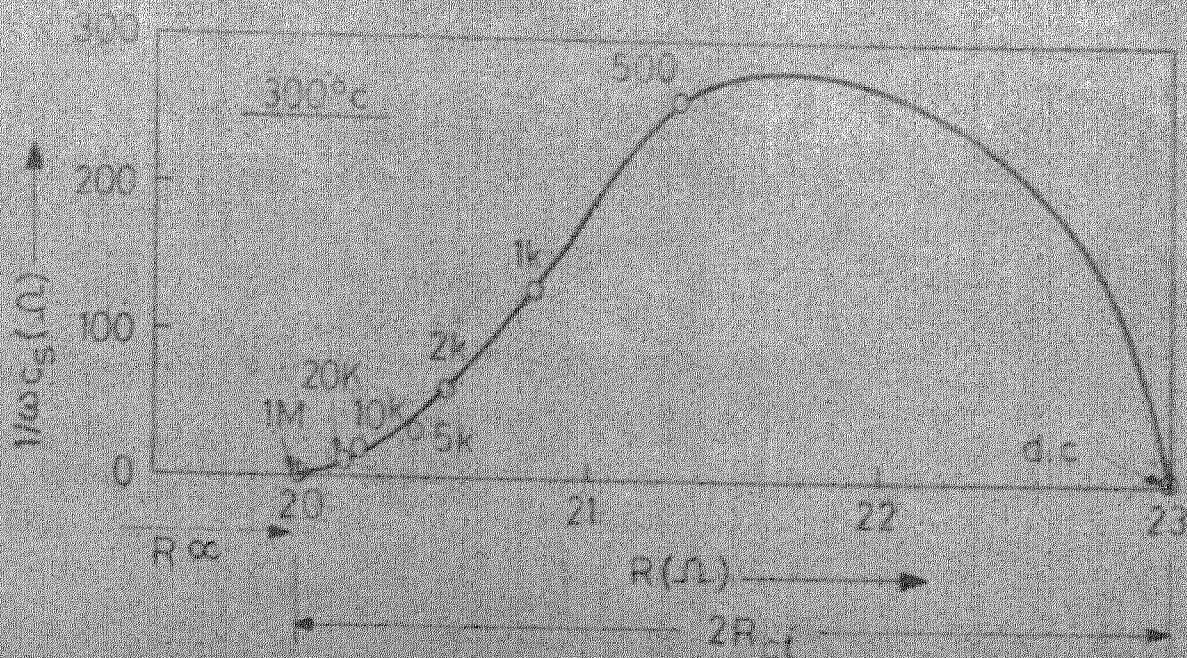


Fig. 8.23. Variation of resistance with frequency for pure β (D) sodium electrodes



Warburg Impedance

(b)

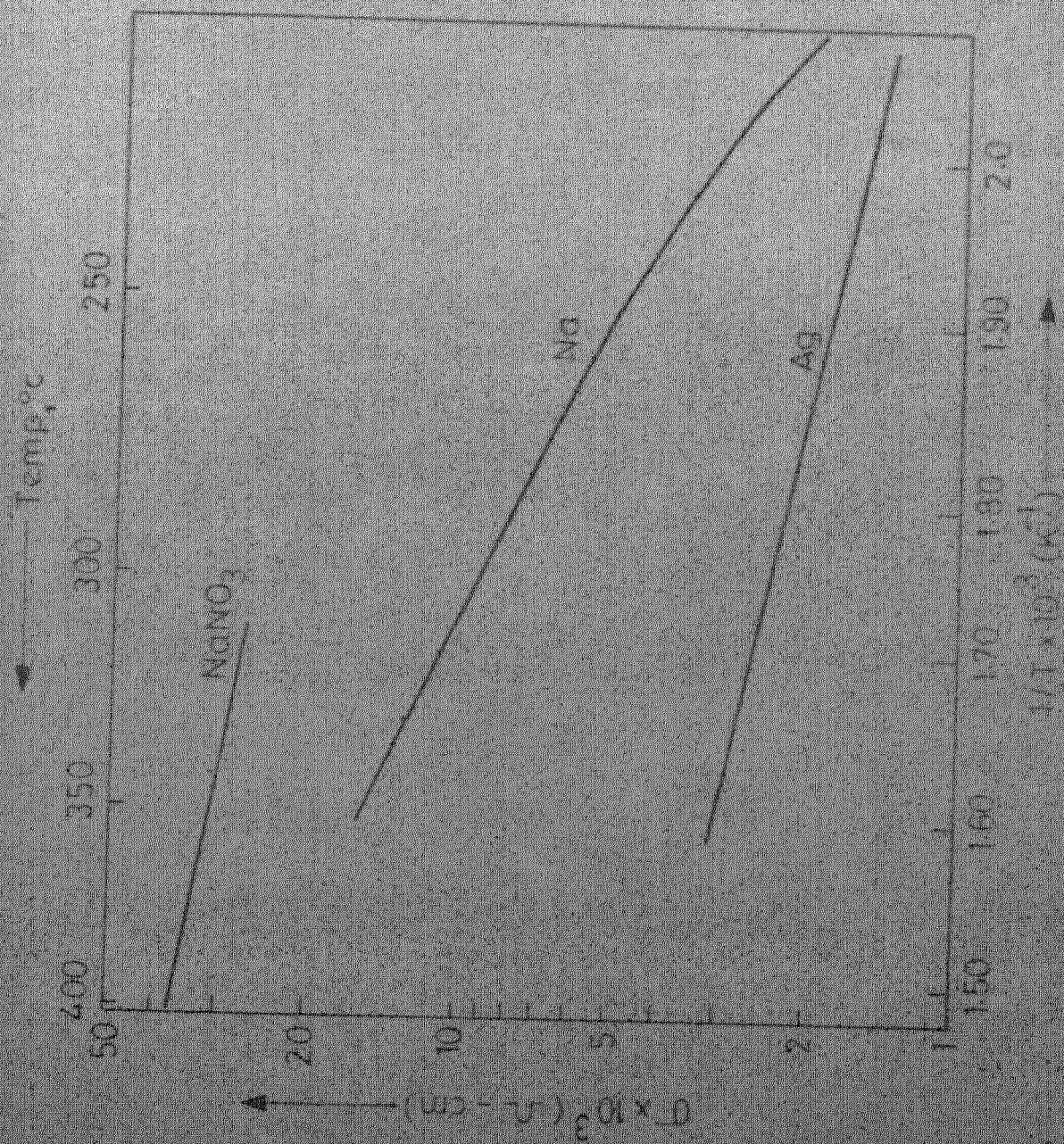


Fig. 1. Temperature dependence of the diffusion coefficient D for NaNO_3 , Na , and Ag in NaNO_3 .

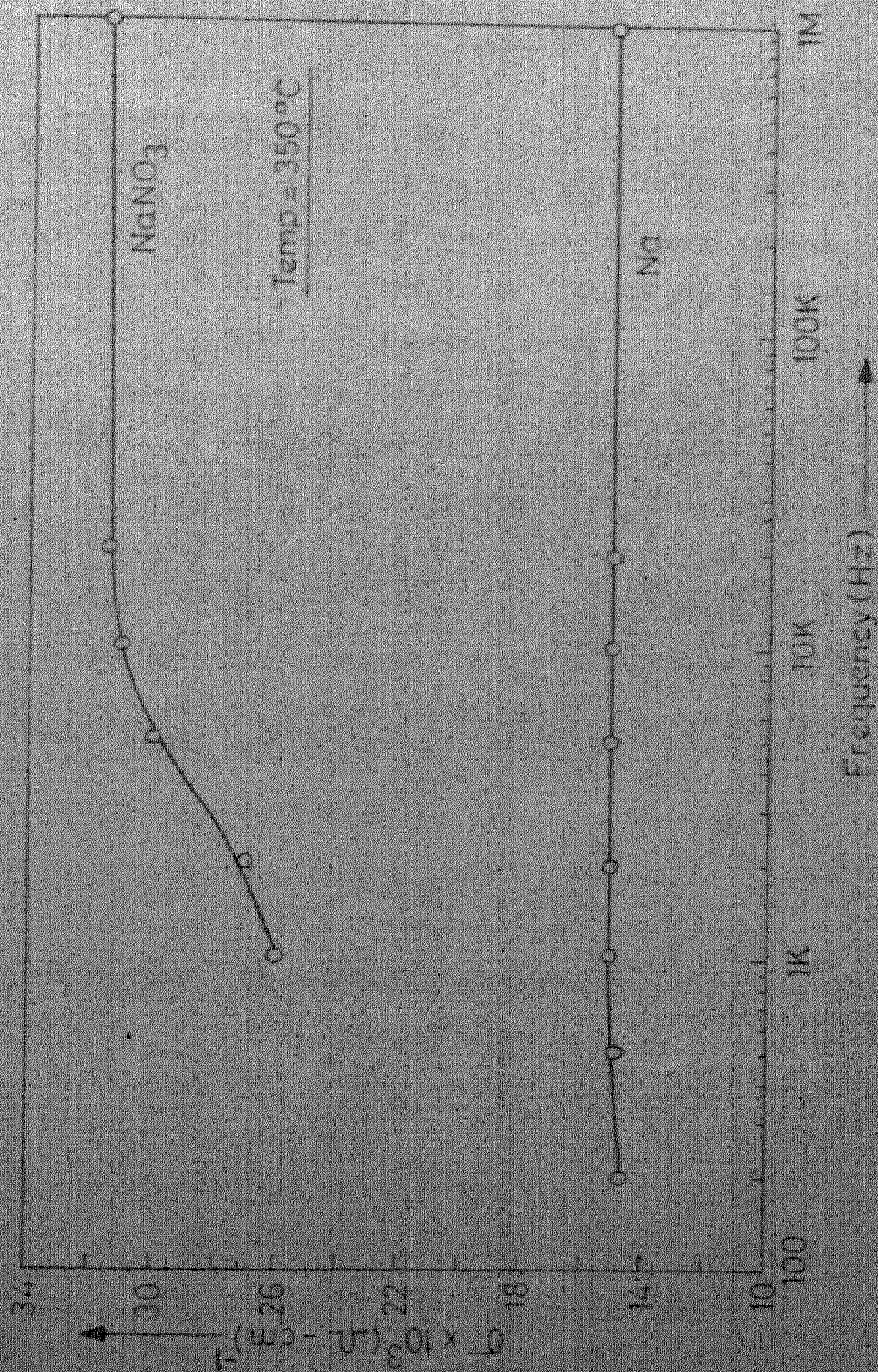


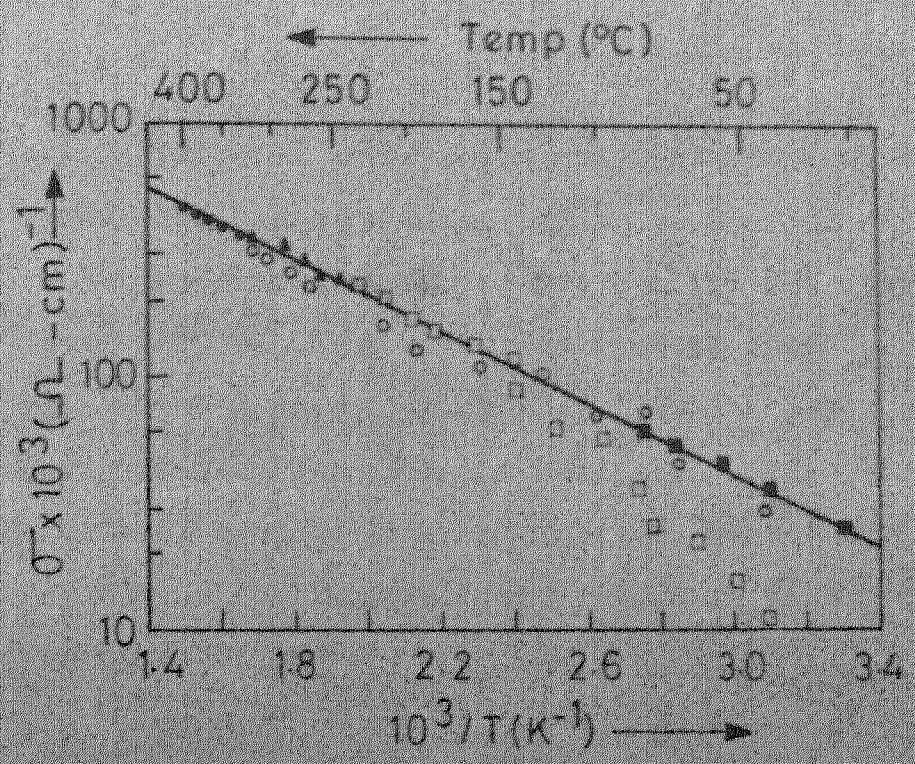
Fig. 1. Comparison of the frequency dependence of the imaginary part of the dielectric constant of NaNO₃ and Na electrodes at 350 °C.

2.1 Electrode Systems

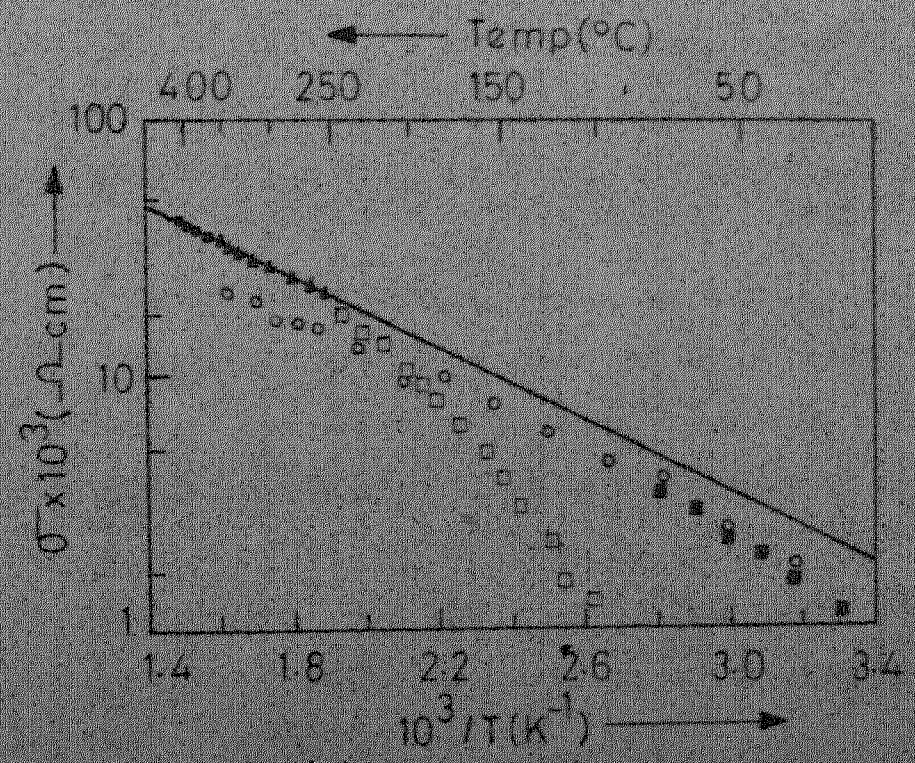
The conductivity values obtained with molten NaNO_3 electrodes are much higher (by about 5-10 times) than those with silver paste, (Fig. 6.1). The values obtained with liquid sodium electrodes are intermediate between these two. NaNO_3 and Na electrodes being liquids are reversible to a large extent, whereas the painted silver electrode is essentially a blocking electrode. Different electrode systems may give different values of conductivity depending upon their nature.

Figure 6.9 shows the results of conductivity measurement by Armstrong et al²⁶ conducted on β -alumina using molten NaNO_3 , molten NaNO_3 - NaNO_2 , evaporated gold, sodium amalgam and aqueous NaNO_3 electrode systems. The straight lines drawn are believed to represent the true conductivity vs. temperature relation. The experimental values agree quite well at high temperatures but diverge from the line at lower temperatures. The molten salt electrodes clearly give a satisfactory contact. The evaporated gold electrode results give a straight line which is parallel to and below the line for molten salt electrodes. The aqueous NaNO_3 results agree well with gold electrode data in the temperature range investigated. The slope of the sodium amalgam results is much larger at lower temperatures. All these divergences from the straight line are smaller in the single crystal case than those in the polycrystalline case.

Other workers have also reported different values for the conductivity of β -alumina using different electrode systems



(a) Single crystal electrolyte



(b) Sintered electrolyte

□ Na / Hg ; ■ Aqueous NaNO_2 ; ○ Au
 ▲ NaNO_3 / NaNO_2 • NaNO_3

Fig. 8.9: Conductivity σ of β -alumina measured with different electrolyte systems.

over a range of frequencies and temperatures. Table 6.6 summarizes these results.

The present measurements confirm the above mentioned facts for the three electrode systems considered. The Ag paste measurements give lower values than the NaNO_3 electrode measurements, but with the same slope. The liquid sodium electrode systems give intermediate values which fall more rapidly at low temperatures. Fig. 6.7 illustrates these facts for composition D.

2.2 Composition

The conductivity of beta-alumina varies to a large extent with the variation in phases present, composition etc. The amount of sodium is, of course, a determining factor. This is evident from the single crystal and polycrystal conductivity data (Fig. 4.3).

The conductivity of β -alumina increases with MgO content. Mg^{++} ions go to the Al^{3+} sites and this necessitates the presence of extra sodium ions in the sodium containing planes for charge neutrality. Thus any increase in MgO content should cause a proportionate increase in the concentration of the moving species. The effect of MgO additions has been studied.^{16,28} It was found that the increase in conductivity is not proportional to the amount of MgO added.

Table 6.6

Conductivity Measurements on β -alumina

Material	Electrode	Frequency Hz	$\sigma \times 10^3$ (ohm-cm) ⁻¹	Temp. °C	Activation Energy kJ/mole	Ref.
Single crystal	Indium	500 k	30 \pm 3	25	11.1	3,6
	"	"	283	300		
	-	-	23	25	14.0	26
	-	-	355	300		
	Na	-	76.5	100	-	34
	Na _x WO ₃	-	14	25	15.8	27
Sintered disc	Aqueous 5M NaNO ₃	1 M	1.84	25	-	26
	NaNO ₃ /NaNO ₂	10 k-1 M	28.5	300	-	"
	Na	d.c.	4.5	25	-	3
	Na	d.c.	55	300	-	"
	Evaporated Ag	0.75-10 k	0.66	25	-	28
	MgO doped (1-4 pct.)	"	3.5-4.4	25	14.6	"
2 pct MgO doped	Na	1592	36	300	13.5	35
MgO doped	Ag	1000	125	350	16.0	17
MgO and ZrO ₂ doped	"	"	200	"	"	"
Pure, β -alumina	Na	20 k	62.5	"	-	33

This suggests that some other phenomenon is involved. Probably beyond a certain limit Mg^{++} ions occupy sites that are not occupied by Al^{3+} ions in the spinel blocks.

For polyphase materials comprising of β and β'' aluminas, the conductivity varies linearly as the percentage of β'' increases.³³ Materials with other less conducting or non-conducting phases should show a further deterioration of conductivity.

The pure β -alumina sample (D) shows the lowest conductivity of the series. Sample E, which contained 1.25 MgO has a higher conductivity, as expected. The conductivity would have been much higher had its density been equal to that of sample D (E has 2.4 as compared to 2.8 gms/cc of D). The conductivities of β'' -alumina specimens A, B and C are higher than those of pure and doped β -alumina, with the conductivity increasing as the extent of doping increases. Sample A with the highest amount of MgO, shows a conductivity of $65 \times 10^{-3} \text{ (ohm-cm)}^{-1}$ compared to a value of $58 \times 10^{-3} \text{ (ohm-cm)}^{-1}$ for sample C at 320°C (as measured with the NaNO_3 electrodes). At the same temperature, the conductivity of pure β -alumina is $28 \times 10^{-3} \text{ (ohm-cm)}^{-1}$. The conductivity of β'' samples thus is about twice that of β sample. The conductivity should have been, however, about one order of magnitude larger on the basis of single crystal conductivity data (Fig. 4.3). Lower density, presence of other phases seem to be responsible for this.

2.3 Temperature

Fig. 6.1 shows the conductivity of all the samples plotted on a $\log \sigma$ vs. $1/T$ diagram. The data obtained from the silver paint measurements fall nearly on a straight line and thus follow the Arrhenius relation. With sodium nitrate electrodes the straight lines observed in $\log \sigma$ vs. $1/T$ plots in Fig. 6.1 exhibit a slight curvature, when the same data are plotted on an expanded temperature scale.

The activation energies calculated for the samples, using Ag paint electrodes (Table 6.1) are nearly the same as the published values (~ 14 kJ/mole for β -alumina)²⁶. The values obtained with NaNO_3 electrodes are slightly lower. The value of the activation energy calculated from the slope of the $\log \sigma$ vs. $1/T$ curves for Na/ β -alumina/Na cell (Fig. 3.4) is about 30 kJ/mole, which is about twice the value obtained from molten NaNO_3 or Ag paste measurements. Similar slopes have been observed by Sudworth, (Fig. 6.10). using purified sodium and oxide saturated sodium with tubes of electrolyte.³³ The liquid sodium electrodes can cover a wide range of temperature (150-400°C), where as molten NaNO_3 system is limited to a range of 320-400°C.

Resistance measurements were carried out on β'' -alumina (sample B) at lower temperatures (upto 125°C) using Ag paste electrodes. The results obtained are plotted in Fig. 6.10. A break in the straight line can be seen at about 180°C, below which the slope is much higher. A similar behavior has

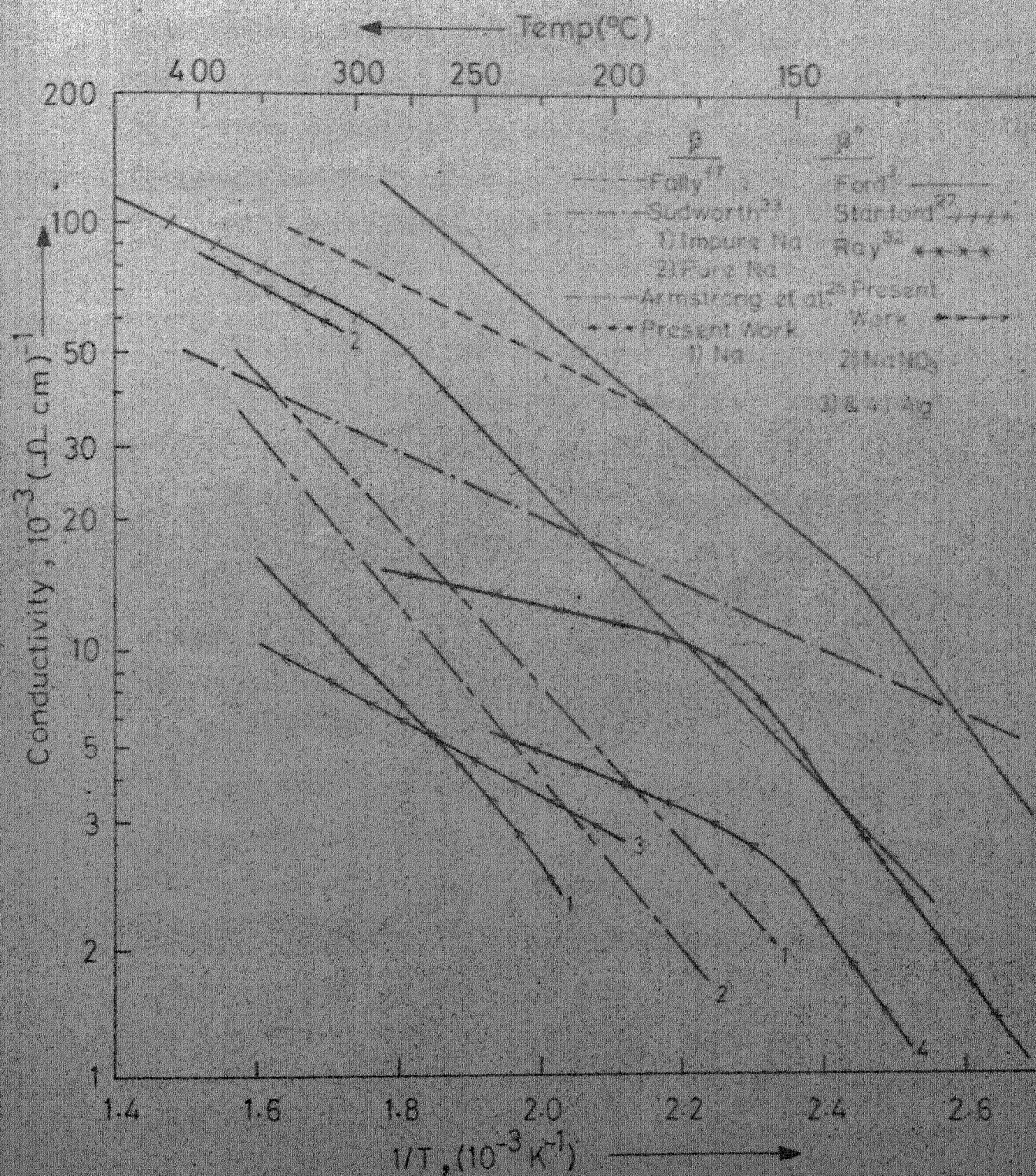


Fig. 6.19: Comparison of the present conductivity data with the reported data

been observed by others (Fig. 6.10) in the case of polycrystalline β'' -alumina samples the break occurring at different temperature depending upon the electrode system and the frequency used. The change in slope is due to the change in the conduction mechanism and is not yet fully understood.

2.4 Frequency

Electrode polarization is one of the most important factors to be considered in the conductivity measurement of 'super-ionic conductors' (see Sec. 2.1 Chap. IV). With blocking electrodes, (silver paste) very high frequencies are needed to avoid polarization. Using these electrodes the resistance of the specimens was observed to be of the order of tens of kilo-ohms at low frequencies (even upto 100 kHz). The measurement was, therefore, carried out at a frequency of 1 MHz, which is fairly high and was easily available. Beyond this frequency, measurement becomes a problem, because of the sophisticated equipment needed, and the lead impedance. The polarization is not absent, however, even at this high frequency, as proved by the fact that the conductivity values obtained with NaNO_3 electrodes are much higher for the same sample compositions.

The frequency dependence of molten NaNO_3 electrode measurements is shown in Fig. 6.2. The frequency dependence does not vary much with temperature as shown by the nature of the curves at 350°C and 400°C . This shows that the system gives a very good contact irrespective of the temperature

(above the melting point of NaNO_3 , $\sim 310^\circ\text{C}$).

The 1MHz value can be taken as the infinite frequency value at least for composition D. In fact, the frequency dependence is an interface phenomenon and depends upon the nature of the surface of the sample. With high density samples, the contact area is clearly defined by the geometric surface area of the sample, and therefore the frequency dependence is small.

The d.c. series capacitance with NaNO_3 electrodes was measured at some temperatures and found to be much larger than the expected values for a flat plate electrode ($\sim 20 \mu\text{F}/\text{cm}^2$). This proves that the effective surface area is larger than the geometric surface area, indicating thereby, that the electrode/electrolyte interface is not sharp, due to the porous nature of the electrolyte. Because of this an interface impedance must come into the picture. Also, since all the samples were not of the same geometric shape, an accurate comparison of the bulk properties can not be done on the basis of these data.

The pure β -alumina sample (D) shows the lowest frequency dependence of conductivity (Fig.6.3). This is because, the specimens had the highest density and hence lowest interface effects. The MgO doped β'' -alumina samples had in general lower densities and show very large frequency dependence of conductivity at low frequencies, because the interface impedance dominates at low frequencies.

In the case of liquid sodium electrodes the frequency dependence is much smaller as shown in Fig. 6.8, which compares

the dependence of conductivity on frequency for Na electrode and NaNO_3 electrode systems at 350°C . The frequency dependence is, however, temperature dependent in this case; as shown by Fig. 6.5. At higher temperatures, the liquid sodium gives an improved wetting, and hence lesser frequency dependence.

3. Na/ β -ALUMINA/Na CELL

With liquid sodium electrodes wetting could be achieved at about 375°C only after 7 hours (Fig. 6.3), although the sodium metal contained oxide which improves the wetting behavior.³³ The specimens could not be polished to a very smooth surface, because of the low density and the high porosity; the liquid sodium thus making contact only at projections on the specimen surface, and reducing the effective area of contact. This causes a reduction in the observed conductivity.

The impedance of the interface contributes to a large extent, as proved by the impedance plane plots (Cole-Cole diagrams), with frequency as a parameter (Fig. 6.6). The shape of the plots suggest an equivalent circuit as shown in Fig. 6.6b.^{31,36} The presence of a Warburg impedance is confirmed, which shows that a diffusive process is responsible for conduction at the interfaces. Since β -alumina has a very high concentration of mobile species - it is a 'super ionic' conductor - in single crystal and highly dense forms, the effect should be due to the presence of semi-infinite pores at the interface. Impedance measurements have been done by others and similar results have

been obtained.^{31,37}

These results prove that the surfaces of the samples should be highly polished to make them 'flat', for making sodium electrode measurements. This necessitates fabrication of fully dense sintered specimens.

4. COMPARISON OF ELECTRODE SYSTEMS

The conductivity plots for sample D, obtained using the three electrode systems have been replotted in Fig. 6.7 for comparison. Molten NaNO_3 is apparently the best of the three considered, although, it is applicable in a narrow temperature range. Compared to the NaNO_3 system the molten sodium system works in a much wider range, and has smaller frequency dependence, (Fig. 6.8) as a result of which lower frequencies are adequate for measurements. The frequency dependence is, however, temperature dependent and effective wetting needs a long time. Also this method requires handling of metallic sodium, which is very difficult.

The silver paste electrodes give polarization even at very high frequencies. The four-probe methods can be used with silver paste^{17,30} or other blocking electrodes (see Sec. 2.1, Chap. IV) to get accurate values of bulk properties, but Mitoff outlined a very elaborate equipment for this purpose. The molten NaNO_3 - NaNO_2 electrode system requires atmosphere control, while increasing the temperature range only by about 50°C. In the molten sodium nitrate case, the temperature

is relatively unimportant as far as wetting is concerned, compared to the liquid sodium case, in which frequency dependence vanishes near 350°C . But this electrode system is more frequency dependent in the lower frequency range, showing the presence of polarization. The sodium ions are not readily available in this case as NaNO_3 has to be electrolysed to yield Na^+ ions. This may give rise to evolution of bubbles of the oxides of nitrogen. Probably the formation of gas bubbles at the face of the electrolyte gives rise to polarization at low frequencies. This bubble entrapment can be avoided by keeping the active surface vertical.²¹ In the present study molten NaNO_3 gave higher values of conductivity than liquid sodium, however, other workers have found the reverse to be true.³³

In view of these facts, the NaNO_3 electrode system is the most attractive system, because of the simplicity of the cell design and the equipment needed. With dense sintered specimens, the method should work satisfactorily at frequency of about 10 kHz. The NaNO_3 electrode system should therefore be preferred. The presently used sample holding technique could be improved for handling of a larger number of samples, by avoiding the sealing that is needed here. Larger rod shaped samples could be used, with pads holding molten NaNO_3 on each end, the cylindrical surface being coated by an insulating material.

5. NaNO_3 ELECTROLYSIS

A total charge of about 1650 coulombs was passed through the cell. After carefully removing the NaNO_3 sticking to its outside surface, the tube was weighed and the increase in mass from the original mass was found out. The difference viz. 0.4 gms, must be the mass of sodium electrolysed and corresponds nearly to the value given by Faraday's Law. Since 1 Faraday (96,490 coul.) of charge should electrolyse 23 gms. of sodium, the mass of sodium electrolysed by 1650 coul. should be about 0.39 gms. The test demonstrates the possibility of producing pure sodium metal electrolytically, and can be used whenever the handling of metallic sodium needs to be avoided.

After the test the electrolyte disc was examined and found to have developed small black regions. No effort was made to confirm whether these are metallic sodium accumulations.

6. SODIUM-SULFUR CELL

The pyrex glass cell fabricated in the laboratory was placed inside a small electrical furnace and heated to 300°C . The internal resistance of the cell was found to be very high (few hundred ohms). The cell exhibited a slight decrease in internal resistance as the temperature was increased to 350°C . The cell was allowed to stay at this temperature with a resistance load connected to its terminals. After a few hours the cell exploded!

The electrolyte disc was found to have cracked into two parts. Conclusive evidence could not be found to pin down the cause of the breakdown. Electrolyte cracking or the failure of the seal could bring about contact between the two compartments of the cell and might have been the cause of the trouble.

It was concluded that the cell fabrication should not be taken up until the electrolyte properties and the sealing techniques are improved.

SUMMARY AND CONCLUDING REMARKS

The conductivity of various MgO stabilized β'' and β alumina samples was measured using silver paste, molten sodium nitrate and liquid sodium electrodes. It was found that the observed conductivity generally varied with the frequency of measurement indicating presence of electrode-electrolyte interface impedance. In this respect the molten sodium electrodes yield relatively frequency independent results although the system attains equilibrium after a long time. Since use of molten NaNO_3 as an electrode system permits simple cell designs, this system appears to have an edge over other systems for purposes of screening electrolyte materials. With liquid sodium electrodes the nature of the electrode-electrolyte interface impedance was determined by making impedance measurements as a function of frequency.

An attempt to make a cell, using a 1 in. disc and a glass assembly failed, as it gave very high internal resistance and ultimately broke down. The presently fabricated material was found to be unsuitable for battery use due to its low electrical conductivity and high porosity. Although the samples did not possess continuous pores, they were not impervious. For use in a battery, a ceramic should be dense and impervious to rule out possibility of diffusion of reactants across it. Even with an almost perfect electrolyte, it is essential to ascertain that it won't crack when used in a cell.

This requires subjecting the candidate material to a test in which the actual life-determining conditions are simulated.

Analysis of a cell design showed that the use of materials having smaller conductivity does not much alter the cell performance if the thickness is kept small. Some sacrifice in performance of a cell due to the use of an electrolyte with higher resistance may be traded off by an improvement in cell life due to the better mechanical properties of the electrolyte.

REFERENCES

1. a) S. Gross, pp 9-25, b) G.H. Gelb, N.A. Richardson, E.T. Seo and H.P. Silverman, pp 178-94; in Proc. Symp. Batteries Tract. and Propul, 1972, R.L. Kerr, Ed., Columbus Section, Electrochem. Soc., Battelle Mem. Inst., Columbus, Ohio.
2. E.H. Hietbrink, J. McBreen, S.M. Selis, S.B. Tricklebank and R.R. Witherspoon in Electrochemistry of Cleaner Environments, John O'M. Bockris, Ed., Plenum Press, New York - London (1972) p 47.
3. J.T. Kummer and N. Weber, a) Automotive Engg. Congress, Detroit, (Jan. 1967), b) Energy Conversion Engineering, The American Society of Mechanical Engineers (1967), p 913, c) Proc. 21st Ann. Power Sources Conf., Atlantic City, N.J., P.S.C., Publications Committee (1967), p 37.
4. N.K. Gupta and R.P. Tischer, J. Electrochem. Soc., 119, 1033 (1972).
5. T.G. Pearson and P.L. Robinson, J. Chem. Soc., 132, 1473 (1930).
6. Y.Y. Yao and J.T. Kummer, J. Inorg. Nucl. Chem., 29, 2453 (1967).
7. J.T. Kummer in Progress in Solid State Chemistry, 7, (1972); H. Reiss and J.O. McCaldin, eds., Pergamon Press, New York.

8. S. Gratch, J.V. Petrocelli, R.P. Tischer, R.W. Minck and T.J. Whalen, Intersoc. Energy Convers. Engg. Conf., Conf.. Proc. 7th (1972), 38-41, ACS, Washington, D.C.
9. R.W. Minck, *ibid.* pp 42-6.
10. J.L. Sudworth and M.D. Hames, Power Sources 3, (1970); D.H. Collins, Ed., Oriel Press (New Castle upon Tyne) pp 227-44 (1971).
11. J.L. Sudworth, Sulphur Inst. J., 8, 12 (1972).
12. J.L. Sudworth, M.D. Hames, M.A. Storey, M.F. Azim and A.R. Tilley, Eighth Internat. Power Sources Symp., Brighton, Sussex, Eng. 26-28 Sept. 1972. (Croydon, Surrey, England; Internat. Power Sources Committee, 1972) pp 1-19.
13. L.J. Miles and I. Wynn Jones, *ibid.*, p 245.
14. J. Fally, J. Richez, Y. Lazzannee and C. Lasne, Fr. Demande 2, 129, 864 (1972).
15. J. Fally and J. Richez, Fr. Demande 2, 140, 318 (1973).
16. J. Fally, C. Lasne, Y. Lazennec and P. Margotin, J. Electrochem. Soc., 120, 1292 (1973).
17. J. Fally, C. Lasne, Y. Lazennec, Y. Le Cars and P. Margotin, J. Electrochem. Soc., 120, 1296 (1973).
18. N.G. Bukun, E.A. Ukshe, N.S. Lidorenko and A.A. Lanin, U.S.S.R. Pat. 366, 517 (1973).
19. I. Wynn Jones in Fast Ion Transport in Solids, W. Van Gool, Ed., North Holland Publishing Co., Amsterdam - London (1973).

20. J.J. Werth, U.S. Pat. 3, 718, 505 (1973).
21. G.J. Tennenhouse, R.C. Ku, R.H. Richman and T.J. Whalen, American Ceramic Society, 75th Ann. Meeting and Exposition, May (1973).
22. R.H. Richman and G.J. Tennenhouse, *ibid.*
23. K.D. South, J.L. Sudworth and J.G. Gibson, J. Electrochem. Soc., 119, 554 (1972).
24. P.D. Greene, Electronics & Power, 18, 395 (1972).
25. M.J. Rice and W.L. Roth, J. Solid State Chem., 4, 294-310 (1972).
26. R.D. Armstrong, T. Dickinson and J. Turner, J. Electrochem. Soc., 118, 1135 (1971).
27. M.S. Whittingham and R.A. Huggins, J. Chem. Phys. 54, 414 (1971).
28. J.H. Kennedy and A.F. Sammells, J. Electrochem. Soc., 119, 1609 (1972).
29. H.E. Kautz, J. Singer, W.L. Fielder and J. Stuart Fordyce, NASA TN. D-7146 (1973).
30. S.P. Mitoff in Fast Ion Transport in Solids, W. Van Gool, Ed., North Holland Publishing Co., Amsterdam - London (1973).
31. R.D. Armstrong, T. Dickinson and J. Turner, Electroanal. Chem. and Interfacial Electrochem., 44, 157 (1973).
32. A.K. Ray, M.Tech. Thesis, I.I.T. Kanpur (Jan. 1974).

33. J.L. Sudworth, A.R. Tilley and K.D. South in Fast Ion Transport in Solids, W. Van Gool, Ed., North Holland Publishing Co., Amsterdam-London (1973).
34. A. Imai and M. Harata, 137th Meeting of the Electrochem. Soc., Los Angeles, May 1970. Abs. No. 277; quoted in Ref. 7.
35. J.L. Sudworth, Private communication referred in Ref. 26.
36. J.E. Bauerle, J. Phys. Chem. Solids, 30, 2657 (1969).
37. M.S. Whittingham and R.A. Huggins in Solid State Chemistry, R.S. Roth and S.J. Schneider Jr., Eds., NBS Special publication No. 364, (1971).

APPENDIX

Intrinsic Efficiency

The Gibbs free-energy change is related to the electrochemical equilibrium potential E , by the following relation:

$$-\Delta G = nFE$$

The total energy change, ΔH in a reaction is, however, always larger than ΔG , and the remaining energy is lost as an entropy increase.

Hence the maximum intrinsic efficiency is given by

$$\eta_{\max} = \frac{\Delta G}{\Delta H}$$

This is in general nearly unity and can be neglected. The entropy increase gives rise to a heat loss, which must be accounted for in designing the cooling system of a battery.

Voltage Efficiency

As soon as a current (I) is drawn from a cell, the cell potential falls from the equilibrium value E to $V = E - I R_{\text{in}}$, where R_{in} is the internal resistance of the cell due to polarization etc. Therefore a voltage efficiency $\eta_v = V/E$ is defined for cell systems.

Faradic or Current Efficiency

The voltage efficiency gives the actual efficiency of a

cell only if the reactants are completely converted to final reaction products i.e., if the overall reaction is fully accomplished and none of the electrons take part in some alternative reaction. To allow for the possibility that such a wastage does occur, a current or faradai efficiency η_f must be taken into account.

$$\therefore \text{Overall efficiency} = \eta_{\max} \cdot \eta_v \cdot \eta_f$$

In many reactions η_f is virtually unity.

Power Output

The power P of an electrochemical convertor is defined as

$$P = IV \text{ (watts)}$$

Energy Output

$$\text{Energy output, } W_o = PT \text{ (watt-hours)}$$

where T is the discharge time in hours. It is assumed that all the stored energy is used up by drawing power uniformly at P for T hours. For large T , P or the current density has to be maintained to a small value.

$$W_o = I(E - IR_{in})T = \eta_d W$$

where η_d = discharge efficiency

W = stored energy

The power P is small, when the current is small, even though the voltage V is near the e.m.f. E . The power output

is also small, when the current is very large because of the growth of the over potentials (IR_{in} term). Thus the P vs. I shows a maxima. For getting a high efficiency, the power must be maintained at a low value. Conversely for a small discharge time, i.e., with high current densities, the efficiency of conversion falls to a low value. At the highest current drains, both the power and efficiency fall to zero.

Energy Density

This refers to the energy which may be extracted from a given mass of reactants or a device per unit mass.

$$\text{Energy density} = nFE \eta_d / M$$

where M is the total mass.

Since η_d is dependent upon the rate of discharge for a certain device, energy density as well as power density are dependent upon rate of discharge.

A 29986

Date Slip A 29986

This book is to be returned on the
date last stamped.

.....
.....
.....
.....
.....
.....
.....
.....
.....
.....
.....
.....

CD 6.72.9

M 8-1974-M-TIK-SOD